J MATER SCI 41 (2006) 873–903

Applications of Secondary Ion Mass Spectrometry (SIMS) in Materials Science

D. S. McPHAIL
The Department of Materials, Imperial College, Prince Consort Road, London SW7 2AZ, England, UK
E-mail: d.mcphail@imperial.ac.uk

Secondary Ion Mass Spectrometry (SIMS) is a mature surface analysis technique with a vast range of applications in Materials Science. In this review article the SIMS process is described, the fundamental SIMS equations are derived and the main terminology is explained. The issue of quantification is addressed. The various modes of SIMS analysis including static SIMS, imaging SIMS, depth profiling SIMS and three-dimensional (3D) SIMS are discussed as are specialized analysis strategies such as the imaging of shallow bevels and cross-sections and reverse side analysis. SIMS is shown to be a useful sample preparation tool based on ion beam milling (with SIMS and Scanning Electron Microscopy (SEM) analysis providing end-point detection). The case studies shown illustrate the application of SIMS to several important materials including semiconductors, superconductors, glass, stainless steel, micrometeoroids, solid oxide fuel cell components, museum artifacts, aerospace alloys and biomaterials. Strategies for introducing SIMS into undergraduate education and thus increasing awareness are described. Finally some informed guesses are made as to the future directions of SIMS.
© *2006 Springer Science + Business Media, Inc.*

1. Fundamentals

1.1. An introduction to the SIMS technique

Secondary Ion Mass Spectrometry (SIMS) is now a mature surface analysis technique having been used for over thirty years, mainly to support the semiconductor industry, where it has been and continues to be used for process development, process monitoring and troubleshooting. But, whilst that one industry has provided the impetus for the development of SIMS instrumentation and methodology, it is now clear that there any many other areas of science and technology where SIMS has an important role to play. In this paper I will review some of the recent applications of SIMS, drawing upon examples that will, hopefully, suggest how the technology and methodology is transferable to yet more areas of materials science.

SIMS is a surface analysis technique with trace element sensitivity, capable of sub-nanometre depth resolution and a lateral resolution of 5 nm. SIMS can be used to measure all elements and isotopes in the periodic table. The experiments are conducted in a vacuum. Three examples of the power of the SIMS technique are shown below. The first example, shown in Fig. 1, is a *SIMS depth profile* in which SIMS is used to determine the composition as a function of depth of six oxynitride films grown under a variety of conditions. This material is being studied as a possible replacement for SiO_2 in transistor gate oxides to reduce the gate leakage and boron penetration that often occurs with SiO_2. The nitrogen concentration is plotted as a function of depth and the depth scale is believed to be accurate to approximately 0.3 nm. Subtle differences in the shape of the nitrogen distribution are observed (image courtesy of FEI, [1]).

Fig. 2 shows the power of *SIMS imaging* where the lateral distribution of elements of interest are measured. SIMS images have been taken at appropriate mass numbers for the polymer, stabilizer and anti-oxidant in a car bumper and the overlay clearly indicates the non-uniform lateral distribution of these three components (images courtesy of ION-TOF [2]).

SIMS depth profiling and imaging may be combined to yield a three-dimensional SIMS chemical map of a material, and an example is shown in Fig. 3. The material shown here is a low-lime glass that is vulnerable to atmospheric attack. Sodium ions diffuse from the bulk of the glass to the surface being replaced by hydrogen ions from the atmospheric water. The sodium map gives insights into the corrosion mechanism. The *3-D SIMS map*

0022-2461 © *2006 Springer Science + Business Media, Inc.*
DOI: 10.1007/s10853-006-6568-x

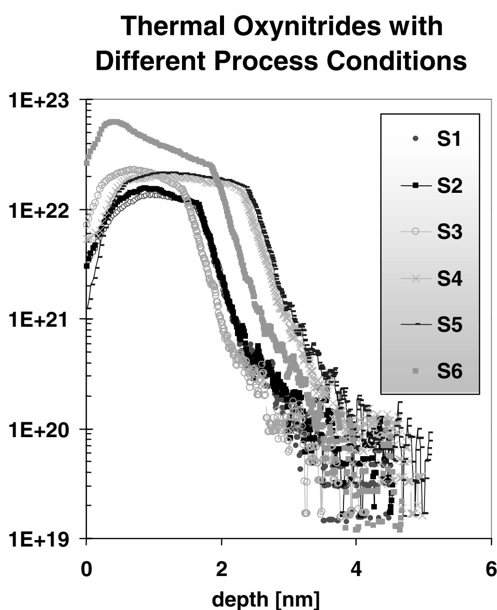

Figure 1 Ultra-shallow SIMS depth profiles of the nitrogen concentration as a function of depth for six oxynitride films that were subject to different processing conditions. The samples were analysed using a 250 eV oxygen beam at an angle of incidence of 70° on an Atomika 4550 at FEI Munich (image courtesy of Dr Hans-Ulrich Ehrke [1]).

has been opened up retrospectively at places of interest to follow the sodium pathway (image courtesy of FEI, [1]).

SIMS is essentially a combination of sputtering and mass spectrometry applied (almost always) to solid surfaces. It is often very useful to take a secondary ion mass spectrum of the sample as a first stage in any analytical protocol, for example to identify the elements of interest or indeed to check that the sample is mounted the correct way up! It is important to recognize, however, that the relative intensities of the secondary ion peaks in SIMS do not directly reflect the relative concentrations of the species in the sample (see the section below on the SIMS process) so that the 'raw' mass spectrum only provides qualitative information. However, the relative intensities of the different isotopes of an element do accurately reflect the relative abundances of those isotopes in the sample, although subtle mass fractionation effects do exist. Examples of mass spectra are given later.

Sputtering is achieved by irradiating the surface of the sample with a beam of energetic ions, usually with ion beam energies somewhere in the range of 250 eV to 30 keV. The primary ion generates an intense but short-lived collision cascade and many atoms of the matrix are relocated. Some of the atoms near the surface receive

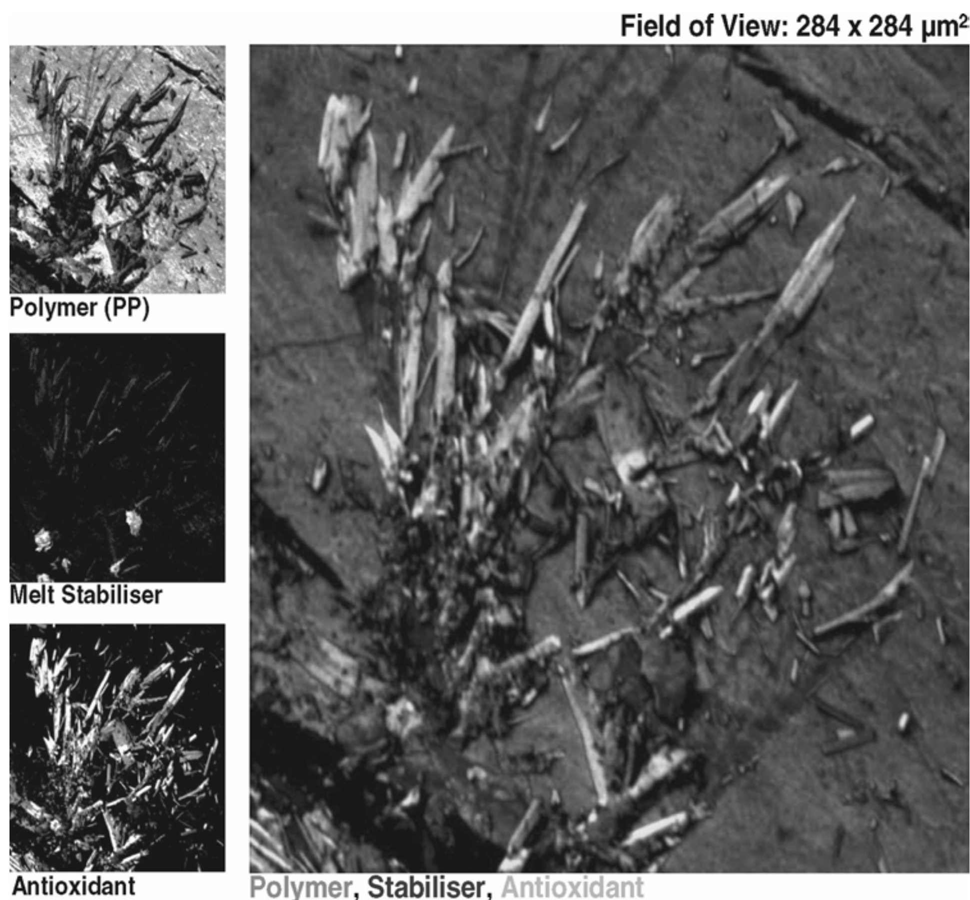

Figure 2 A blooming effect on a car bumper. TOF SIMS images of three components, namely the polymer, stabiliser and antioxidant, in a sample from a car bumper, and an overlay showing their relative distributions (image courtesy of Mr. Colin Helliwell ION-TOF, [2]).

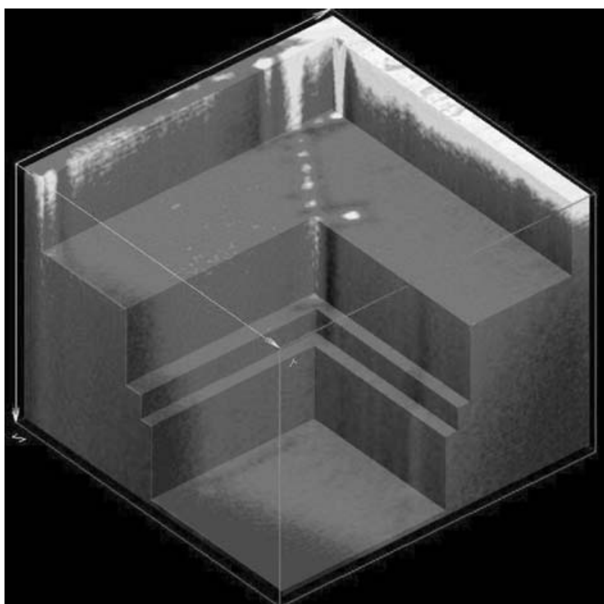

Figure 3 A three-dimensional image of the sodium distribution in a glass, following analysis on an Atomika 4550 SIMS instrument. Retrospective data processing has been used to 'open-up' the structure to reveal aspects of interest in the sodium distribution (image courtesy of Dr. Hans-Ulrich Ehrke, FEI, [1]).

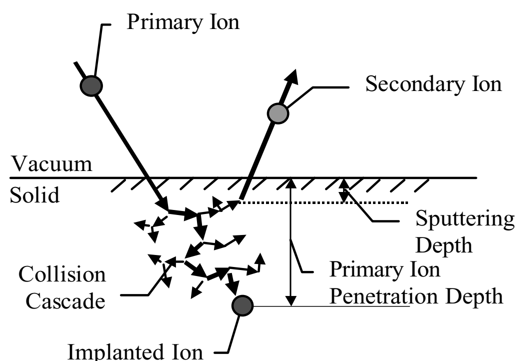

Figure 4 The collision cascade in SIMS. The primary ion finally comes to rest after a series of collisions during which displacements of the sample atoms occur. Some secondary species are ionised and it is these secondary ions that are of use. Typically the range of the primary particle is 1–20 nm in a SIMS experiment, depending on the primary beam energy used.

enough energy to leave the surface; these are the sputtered atoms (Fig. 4). The dimensions of the cascade and the range of the primary ions have been modeled and commercial software (profile code TRIM and SRIM) [3] is now available to generate visual displays of the cascade and to give key parameters such as the range and straggle of the primary ion. One useful formula gives the range of oxygen ions in silicon [4] as:

$$R(\text{nm}) = 2.15\text{E}(\text{keV})\cos(\theta)$$

R is the vertical range in nanometres; E is the energy of the primary ion (in keV) and θ the angle of incidence with respect to the surface normal. A 10 keV O^+ ion at normal incidence will have a range of approximately 21.5 nm in silicon and to a first approximation this is the scale of the collision cascade and also an indication of the 'depth resolution' achievable (see below). The range at 1 keV will be 2.25 nm, and at 250 eV approximately 0.5 nm. By working at a grazing angle of incidence of 80° it is possible to reduce the range by a factor of 5.8. Thus at sub-keV energies the collision cascade can be approximated as a hemisphere with sub-nm dimensions thus minimizing the beam induced mixing processes and leading to the possibility of sub-nanometre depth resolution. Heavier primary ions will have lower ranges and one of the latest ion sources now available uses a ${C_{60}}^+$ primary ion [5]. This species disintegrates when it arrives at the sample surface thus all its energy is dissipated into the top few surface layers (furthermore there is no possibility of ion channeling as the primary ion is too large).

As mentioned above some fraction of the atoms in the collision cascade will be able to escape the surface, and this is the basis of sputtering. Typically these atoms have an energy distribution that peaks at about 10 eV. Thus the surface atoms will be removed either as atomic or molecular species and the material under investigation will be gradually eroded. The key observation (first made by J.J. Thomson in 1910, [6]) is that some fraction of the atomic and molecular species leaving the surface will be electrically charged (positively or negatively) and can, therefore, be entrained by electric and/or magnetic fields and transmitted to a mass spectrometer for mass analysis. The information depth in SIMS is believed to be essentially the top two or three atomic layer [7, 8] so that monolayer depth resolution is, in principle, possible in SIMS. In practice the ions are usually being emitted from a region that has been 'mixed-up' by previous collision cascades so that sub-surface atoms will have been transported to the surface and will form part of the secondary ion signal. This is not true if the primary ion dose is less than $\sim 10^{13}$ primary ions/cm^2 and in this regime, where each primary ion impact is on virgin surface, true monolayer sensitivity is achievable (the Static SIMS regime).

The basic experimental set-up is shown in Fig. 5. The ions being used to effect the sputtering are termed the 'primary ions' and the ions being sputtered are termed the 'secondary ions'. The primary ions implanted into the sample surface physically and (sometimes, depending on the species) chemically modify that surface, and these changes to the surface due to the interaction with the primary ion beam are of the utmost importance in SIMS in determining the probability that the sputtered flux is ionized (the ionization probability). Under steady state sputtering conditions the rate of implantation of primary species is equal to the rate at which they are sputtered. Since the sputtering is essentially a surface phenomenon any species from the residual vacuum arriving on the surface being analysed will be sputtered as well, often compromising the detection limits of the analysis or making

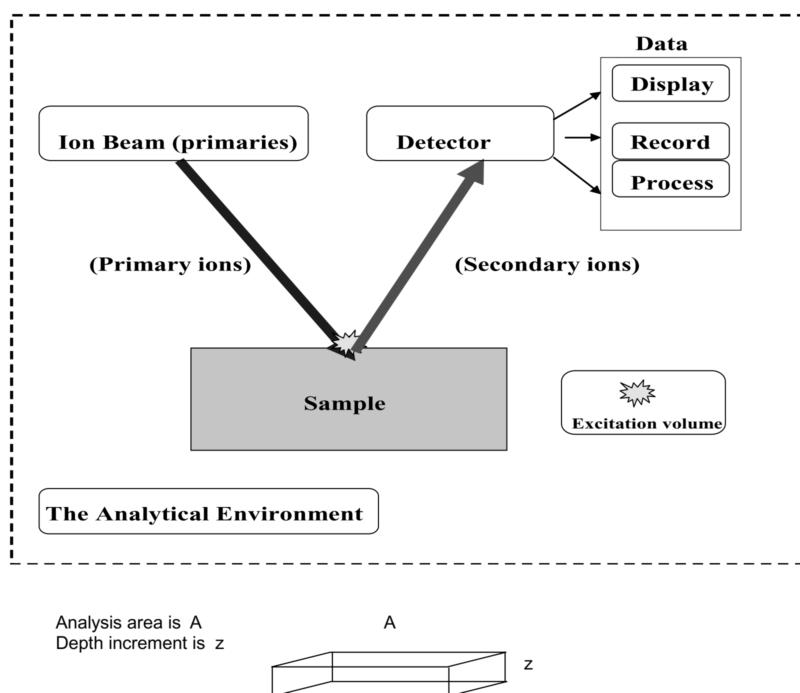

Figure 5 The fundamentals of SIMS analysis. The SIMS Process: The probe is an energetic beam of primary ions. Beam currents are usually in the pA-μA range and beam energies in the range 250 eV to 30 keV. The angle of incidence (with respect to the surface normal) is an important analytical parameter. The sample is irradiated with the primary ion beam, which is often scanned over the surface, to generate a flat-bottomed crater and sputtering leads to the emission of secondary ions. Analysis of the secondary ions involves a mass spectrometer and a detector. The quality of the vacuum is an important consideration.

interpretation of the secondary ion mass spectrum more difficult, thus the quality of the vacuum can be very important. The primary ions can channel if the sample is crystalline (and remains crystalline during ion bombardment) and the lattice oriented in the correct direction. Ion beam channeling contrast is an excellent method of yielding contrast between grains in different orientations. The analytical output in this technique is the intensity of the secondary ion and this can be displayed in real time, as well as being stored for subsequent data processing. It is important that the secondary ion extraction field is invariant during the analysis; unfortunately however the sample may charge-up during the analysis if the charge deposited by the secondary ions is not effectively and rapidly discharged and then the surface potential will change. Methods of charge compensation include gold coating and simultaneous irradiation with a low-energy electron 'flood' gun.

1.2. The SIMS process, SIMS definitions and SIMS equations

1.2.1. The fundamental SIMS equation

The fundamental SIMS equation is deceptively straightforward, and is the basis of the quantification process, but the 'devil is in the detail'. The basic situation, illustrated in Fig. 5 shows the ion beam being used to remove a volume element of material (Az) during a sputtering time t, where A is the area of material being analysed and z the depth of material removed. We will assume for the sake of simplicity that the material is made of only of matrix atoms type M, containing some impurity atoms type X.

Thus the analytical volume removed:

$$V = Az \tag{1}$$

If the average concentration of the species of interest 'X' (X = impurity) in this analytical volume is given by ρ_X then the number of atoms type (X) sputtered is given by:

$$N_X = \rho_X(Az) \tag{2}$$

Importantly it is assumed here that all the atoms of type 'X' within the elemental volume are sputtered although relocation events due to ion beam mixing are important in SIMS as we will see later.

The impurity atoms can leave the surface in many different forms, for example as atoms X, dimeric or higher order polymeric species Xn, polymeric species formed by X with matrix atoms M (M_aX_b) and or with ion beam species type I (i.e. $M_aX_bI_c$), where a, b and c are integers. Obviously the situation and the associated spectra can become very complicated when complex matrices containing many dopants are involved; furthermore the

spectrum will contain contributions from all the isotopes of all the atomic constituents.

The key point is that some fraction of these sputtered species will be ionized. If we consider by way of example the atomic positive ion X^+ then the number of ions of this type that are generated is given by:

$$N_{(X^+)} = \alpha_{(X^+)}\rho_X(Az) \tag{3}$$

where $\alpha_{(X^+)}$ is the ionisation probability for this particular species, defined as the fraction of the atoms X that are generated as atomic ions type X^+. The ionisation probability is the same for each isotope.

The number of secondary ions that will actually pass through the mass spectrometer and be detected will depend on the efficiency of the secondary ion optics and the detector. These factors are collectively known as the secondary ion transmission coefficient T. Thus the number of ions type X^+ actually detected $N^*_{(X^+)}$ are given by:

$$N^*_{(X^+)} = \left(\alpha_{(X^+)}\ T_{(X^+)}\right)\rho_X\ (Az) \tag{4}$$

There is no successful theory that accurately predicts the values of ionization probabilities; furthermore secondary ion transmissions can vary from day to day on the same instrument, depending on the analysis conditions, so it is necessary to measure the unknowns experimentally. It is not normally possible to measure $\alpha_{(X^+)}$ and $T_{(X^+)}$ independently, but their product $Y_{(X^+)}$ is called the 'useful ion yield', for the species in question (X^+) in this case, and this can easily be measured with standards.

$$Y_{(X^+)} = \alpha_{(X^+)}\,T_{(X^+)} \tag{5}$$

$Y_{(X^+)}$ is the useful ion yield for (X^+). The useful ion yield for X^+ is the ratio of the number of secondary ions detected to the number of atoms type X sputtered. Typically it will be measured by analysing an ion-implanted standard of known dose and comparing the number of type X atoms sputtered to the number of ions type X^+ detected. A typical result for boron in silicon is $\sim 10^{-3}$ under favourable analysis conditions [9]. Equation 4, which I will refer to as 'the SIMS equation' can also be written in terms of rates with the number of ions type X^+ detected per second written as $N^{*\prime}_{(X^+)}$ and the rate of sputtering as z', i.e.

$$N^{*\prime}_{(X^+)} = \left(\alpha_{(X^+)}\,T_{(X^+)}\right)\rho_X(Az') \tag{6}$$

$N^{*\prime}_{(X^+)}$ is often found written in the literature as I or I_s.

1.2.2. The sputter yield

The rate of sputter removal of material in SIMS is encompassed in the sputter yield, S, defined as the number of atoms of the material removed, per incident primary species, thus

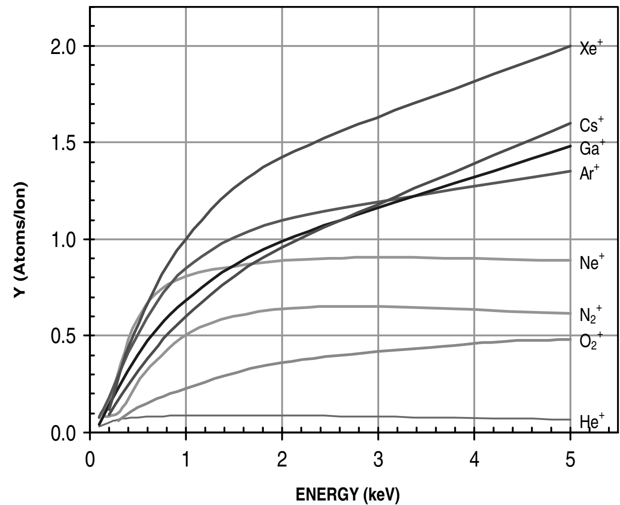

Figure 6 The sputter yield of silicon as a function of beam energy. The data is shown for beams incident normally on the sample surface between 0 keV and 5 keV. Data courtesy of Ionoptika [10].

$$S = \{\rho_M\,(Az)/(I_p/e)t\} \tag{7}$$

where ρ_M is the concentration of matrix atoms, I_p the primary beam current and e the elementary charge on the electron. Sputter yields tend to be in the range 0.1 atoms per ion to 10 atoms per primary ion. The sputter yield of silicon, irradiated with a variety of primary ion beams, is shown by way of example, in Fig. 6 (data courtesy of Ionoptika [10]). Sputtering becomes less efficient below primary beam energies of 1 keV.

From the analyst's point of view the important parameter is the rate of sputtering $z' = (dz/dt)$, which is derived from Equation 7:

$$z' = (SI_p/\rho_M\,Ae) \tag{8}$$

so that the rate of sputtering of the material is determined by the sputter yield, the primary beam current, the atomic concentration of the matrix and the analytical area.

1.2.3. The quantification issue in SIMS

Quantification in SIMS involves the process of converting secondary ion counts or count-rates into concentration. From Equation 6, the SIMS equation, and Equation 5 we can write:

$$\rho_X = N^{*\prime}_{(X^+)}/(\alpha_{(X^+)}\,T_{(X^+)}A\,z') \tag{9}$$

The 'quantification issue' in SIMS arises because the ionisation probability is different for every element 'X' in every matrix M and also depends upon the beam type I

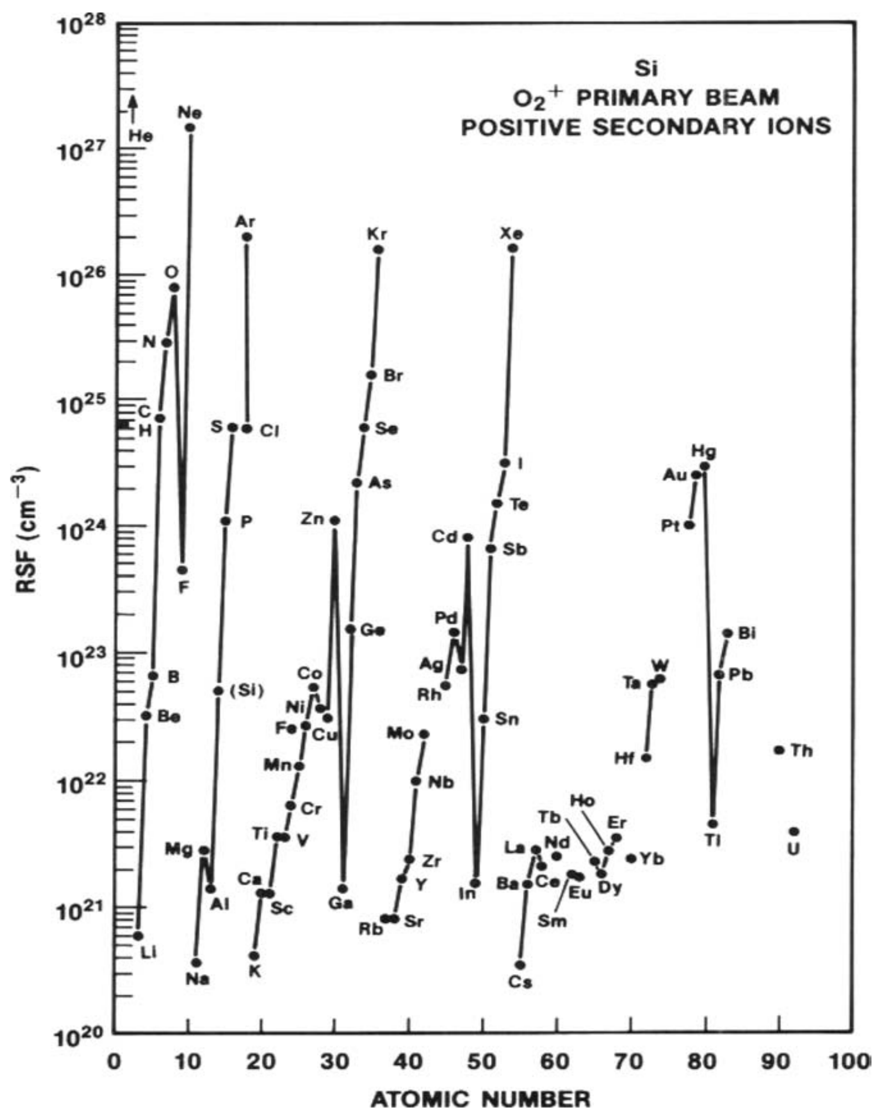

Figure 7 The relative sensitivity factors of the elements. The variation of positive ion yield as a function of atomic number O_2^+ bombardment [11].

used for the analysis, the beam energy E and the angle of incidence of the primary beam with respect to the surface normal θ. α is given by:

$$\alpha_{(X^+)} = \alpha_{(X^+)}(X, M, I, E, \theta) \tag{10}$$

The secondary ion transmission $T_{(X^+)}$ can also vary from one species to another, but this is usually a minor effect. It follows that for a full quantification of a SIMS analysis it is necessary to measure the useful ion yield for each dopant-matrix combination and so it is necessary to have a standard. Thus, for example to analyse for three dopants in a silicon-germanium multi-layer with five different layers, 15 standards are required. The standards must be analysed under the same analytical conditions as the unknown. This is the main drawback of the SIMS technique.

The seminal text book on SIMS, written in 1989 by Wilson, Stevie and Magee [11] shows plots of the 'Relative Sensitivity Factor' RSF of various dilute dopants in semiconducting matrices (silicon and gallium arsenide). The RSF parameter is related to the useful ion yield. A review of quantification procedures using the RSF and RUY (Relative Useful Yield) approach has been given by Douglas Phinney [12]. The important experimental observation is that the useful ion yields for the first 90 elements in the periodic table vary by up to seven orders of magnitude (Fig. 7). Thus for impurities in silicon, analysed with an oxygen primary ion beam, the useful ion yield of sodium (Na^+) is four orders of magnitude lower than that of chloride (Cl^+), reflecting the lower ionization potential of sodium. The converse is also true, the useful ion yield of sodium (Na^-) is four orders of magnitude lower than that of chloride (Cl^-), when analysed with a caesium beam, reflecting the higher electron

affinity of chlorine. Thus judicious choice or primary ion beam type is a very important aspect of experimental design.

The rule of thumb is that elements on the left-hand side of the periodic table tend to form positive ions and this tendency can be increased by irradiating the surface with an oxygen beam, whereas elements on the right-hand side of the periodic table tend to form negative ions and this tendency can be increased by irradiating the surface with a caesium beam.

In a depth profile where the secondary ion intensities are monitored as a function of depth, it is necessary to measure the crater depth to facilitate conversion of the '*x*' axis from time to depth. However, in a multilayer depth profile analysis it is necessary to take account of the different sputter yields of the different layers and to develop a protocol for dealing with the changes in sputter rate across all the interfaces [13]. The depth scale is in effect 'stretched or compressed' for each layer. Furthermore the different sputter rates of the different layers must be accounted for in Equation 9, when converting the intensity scale to a concentration scale.

1.2.4. The relationship between the analytical volume and the sensitivity of the analysis

An issue of obvious concern for the SIMS analyst, as the length metric in semiconductor VLSI technology decreases and new challenges in nanotechnology arise, is the relationship between the sensitivity of the analysis and the analytical volume, or more crudely, "at what point will the technique run out of steam?" For example, the International Technology Roadmap for Semiconductors 2004 suggests that the gate length in transistors will have shrunk to 28 nm by 2009, from 65 nm in 2003 [14].

The fundamental SIMS Equation 4 above

$$N^*_{(X^+)} = (\alpha T)\,\rho_X\,(Az)$$

May be re-written

$$N^*_{(X^+)} = Y\,\rho_X\,V \tag{11}$$

where Y is the useful ion yield for X^+ and V the analytical volume removed during the collection of this data point.

The sensitivity of the analysis is defined as that concentration $\rho_{X,\min}$ that yields a certain threshold number of counts. There is no consensus about the threshold. One hundred counts, corresponding to a statistical uncertainty on the measurement of the concentration of 10%, will be used here. Thus the concentration of impurity that corresponds to the threshold sensitivity is given by:

$$\rho_{X,\min} = 100/(YV) \tag{12}$$

In order to have a good sensitivity to an impurity X in a matrix M, we should have a large useful ion yield (ideally unity) and a large analytical volume. If we assume that the useful ion yield is 10^{-3}, a best case scenario, then the sensitivity (atoms of impurity/m^3):

$$\rho_{X,\min} = (10^5/V)\,(\text{at/m}^3) \tag{13}$$

The sensitivity of the analysis $\rho_{X,\min}$ is shown in Table I as a function of analytical volume V. Normally the useful ion yield in the analysis will be between 10^{-3} and 10^{-6} so data are given for this range, with a column showing the situation were it possible to have a useful ion yield of 1, i.e. the theoretical minimum concentration that SIMS could detect in the 'perfect' instrument with 100% ionization and transmission. If the matrix is present at 10^{29} atoms/m^3 then we note that parts per billion (ppb) sensitivity corresponds to atomic concentrations $<10^{20}$ at/m^3, parts per million (ppm) sensitivity corresponds to atomic concentration $<10^{23}$ at/m^3, and parts per thousand (ppt) corresponds to atomic concentrations $<10^{26}$ at/m^3.

SIMS cannot be used to measure trace level impurities from very small analytical volumes, and to achieve such sensitivities the analytical volume must be increased by increasing the 'box' dimensions in one or two dimensions. Fig. 8 is a graphical representation of the trends shown in Table I, showing the relationship between sensitivity, analytical volume and useful ion yield.

Classical SIMS analysis has involved in-depth analysis or depth profiling where the beam is scanned over a large area and the depth increment per data point is small. For a 100 μm crater (10^5 nm on side) a depth increment of 1 nm per data point will yield an analytical volume of 10^{11} nm^3 so that an impurity concentration of 10^{21} at/m^3 would yield 100 counts, assuming $Y = 10^{-3}$. If the matrix concentration is 10^{29} at/m^3 this corresponds to a sensitivity

TABLE I The sensitivity $\rho_{X,\min}$ achievable in SIMS as a function of the analytical volume V and useful ion yield Y for the impurity in question

$\rho_{X,\min} = 100/(YV)$				
Box edge (nm)	10,000 nm	1,000 nm	100 nm	10 nm
Box volume (nm^3)	10^{12} nm^3	10^9 nm^3	10^6 nm^3	10^3 nm^3
Y = 1	10^{17}	10^{20}	10^{23}	10^{26}
Y = 10^{-3}	10^{20}	10^{23}	10^{26}	10^{29}
Y = 10^{-4}	10^{21}	10^{24}	10^{27}	(10^{30})*
Y = 10^{-5}	10^{22}	10^{25}	10^{28}	(10^{31})*
Y = 10^{-5}	10^{23}	10^{26}	10^{29}	(10^{32})*

*Not physically meaningful results (units of impurity atoms per m^3).

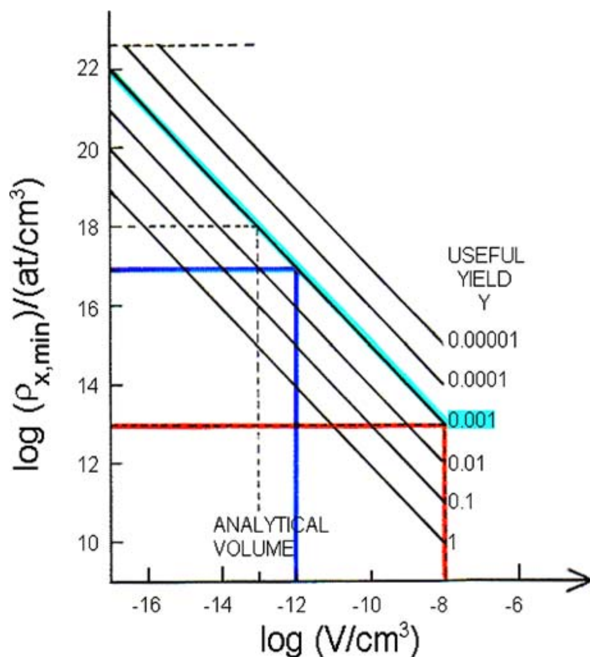

Figure 8 A graph of the variation in SIMS sensitivity with analytical volume for various useful ion yields. The plot indicates log ($\rho_{X,min}$) as a function of log (V) for various useful ion yields Y. $\rho_{X,min}$ is in at/cm^3 and V in cm^3. With a useful ion yield of 10^{-3} and an analytical volume of 10^{-12} cm^3, the sensitivity of the analysis is 10^{17} at/cm^3 (blue line). This corresponds to one part per million, if the concentration of matrix atoms is 10^{23} at/cm^3.

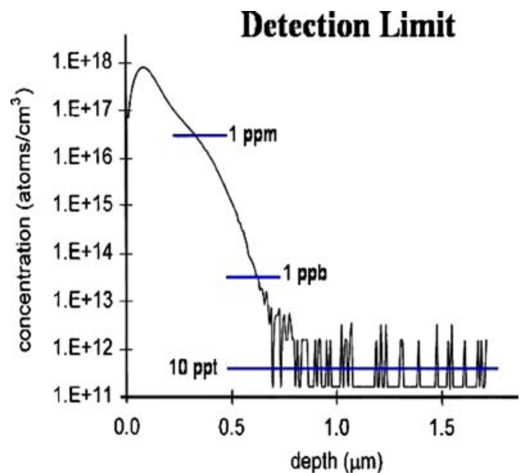

Figure 9 A SIMS depth profile of a low-dose potassium implant into silicon showing a dynamic range of over six orders of magnitude and a discernible profile shape down to a concentration of 10 parts per trillion of potassium in silicon. The data was taken on a Cameca IMS 6F using an oxygen primary ion beam and is courtesy of Fred Stevie in the proceedings of SIMS X1 p983 (see [17]).

of 1 part in 10^8 or 10 parts per billion. This quick calculation shows the reason for the phenomenal success of SIMS depth profiling in measuring trace contaminants as a function of depth. Fig. 9 is a depth profile of a low-dose potassium implant in silicon, conducted by Stevie *et al*. on a Cameca IMS 6F using an oxygen primary ion beam. The implant profile can be followed over more than six orders of magnitude of concentration (the dynamic range) from 10^{18} atoms/cm^3 to approximately 5×10^{12} atoms/cm^3 (or ten parts per trillion).

SIMS imaging is more problematic. If the image area is reduced to a 100 nm square, close to the minimum beam width currently available on imaging instruments, then it is necessary to sputter to a depth of 10^5 nm (100 μm) to remove an analytical volume of 10^9 nm^3 and achieve parts per million sensitivity (with a useful ion yield of 10^{-3}). This is totally impractical since almost no secondary ions would be able to escape such a hole due to the unfavourable aspect ratio! SIMS imaging tends to be used to measure somewhat higher concentrations, for this reason. 'One-dimensional' imaging can be achieved by sacrificing the lateral constraints in one of the surface coordinates.

In all the examples given above it should be noted that we are assuming a useful ion yield Y of 10^{-3} ions detected per atom sputtered. The yield in imaging experiments is often lower; as the ion sources used (i.e. Ga) do not optimize the ionization probability in the same way as the oxygen and caesium guns.

1.2.5. Mass resolution

SIMS involves mass spectrometric analysis and it is important to note that mass spectrometers separate charged particles according to their mass to charge ratio (M/Q), so that for example the species $^{28}Si^{++}$ and $^{56}Fe^{++}$ will appear at the same nominal mass number (28) in the mass spectrum for positive or negative ions. It is also important to note the possibility of other mass interferences, for example at mass 28 we might observe interference due to $C_2H_4^+$, CO^+ and AlH^+, for example. These mass interferences may be resolved on the basis of the subtle differences in their masses, if the *mass resolution* of the instrument is sufficient. Further classic SIMS mass interferences are between $31P^+$ and $^{30}SiH^+$ and between As^+ and $^{29}Si^{30}Si^{16}O^+$. Two masses (M and M+ΔM) are said to be just separated if there is a 50% valley between the peaks.

For example the mass resolution required to separate P (30.973762) from $^{30}SiH^{\pm}$ ($29.973770 + 1.007825 = 30.981595$) $= (30.973762/7.833 \times 10^{-3}) = 3954$. High mass resolution SIMS instruments are designed to split these mass interferences and, for example, a mass resolution of 11,500 is quoted for the TOF-SIMS 5 time-of-flight SIMS instrument (see TOF SIMS 5 Performance Specifications manual, October 2003, [2]). Fig. 10 shows the splitting of $^{56}Fe^+$ and $^{28}Si_2{}^+$ and of $^{63}Cu^+$ and $^{28}Si^{35}Cl^+$ in a time-of-flight secondary ion mass spectrometer. It should be noted that in geology there are many important

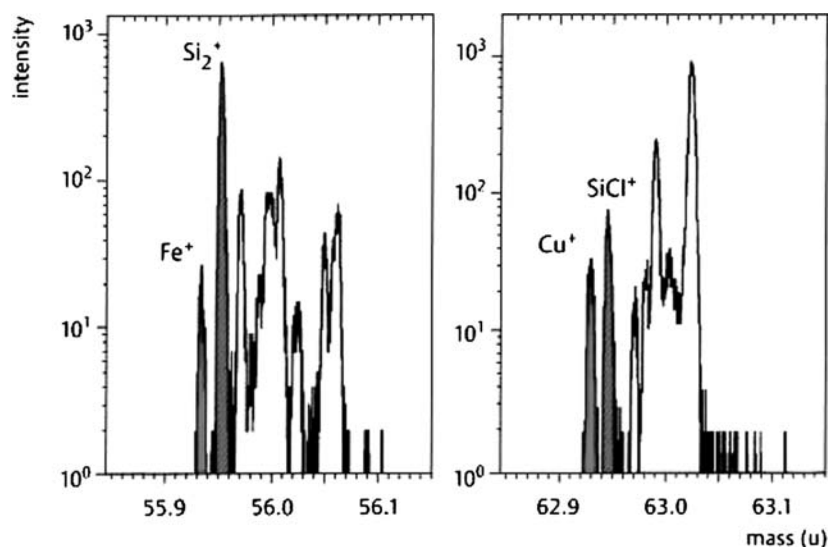

Figure 10 Examples of high mass resolution from an ION TOF 5 instrument, courtesy of Mr Colin Helliwell. This instrument uses a time-of-flight mass spectrometer and can achieve mass resolutions in excess of 10,000 [2]. The examples shown are from an analysis of a silicon wafer. The available mass resolution is sufficient to split the iron signal $^{56}Fe^+$ from the interference due to $^{28}Si_2{}^+$ and the $^{63}Cu^+$ signal from the interference due to $^{28}Si^{35}Cl^+$.

mass-interferences in the radioactive decay series due to mineral hydration.

1.3. Modes of analysis and types of instruments in SIMS

There are two main modes of analysis in SIMS, static and dynamic. For static SIMS the data is typically presented as mass spectra, although imaging can also be of value. For dynamic SIMS, the data can be provided as mass spectra, depth profiles and images. There are several variations on these themes including three-dimensional SIMS, analysis of cross sections and analysis of bevels which will be described in the case studies. The primary ion beam in a SIMS instrument can also be used for sample preparation for other analytical techniques, with SIMS and SEM end-point detection and these will also be described through case studies later. In order to understand the modes of analysis it is first necessary to understand the different types of primary ion columns and secondary ion mass spectrometers available.

1.3.1. Primary ion columns

SIMS instruments and SIMS experiments are defined by the primary ion column(s) used and the type of secondary ion mass spectrometer employed.

Ion columns are designed with imaging experiments, static SIMS experiments or sputtering experiments in mind. With the recent development of the $C_{60}{}^+$ source damage minimization is also re-emerging as a topic of interest so that the possibility of removing large organic/biological molecules essentially intact is becoming a possibility [5].

The best beam widths to date have been achieved using primary ion columns with liquid metal ions sources based on gallium, indium, gold (which can yield gold ions or gold clusters Au_2 and Au_3) and bismuth (which can yield bismuth clusters Bi_2, Bi_3). Binary alloys such as AuGe, AuSiBe and AsPd have also been used. These liquid metal sources generate ions by field evaporation from the ‘Taylor cone’ formed at the tip of a sharp needle [14, 15]. The metals are chosen because they can form a liquid meniscus at the tip of the needle leading to a very well defined source of primary ions, and thus to a beam width at the sample surface of ~50 nm with 5 nm possible in a dedicated FIB instrument. Unfortunately interaction of these metals with the sample do not lead to good ion yields. The efficiency of these sources appears to improve with the mass of the primary ion species as shown above (Fig. 11 from Ion TOF). These sources normally generate beam currents in the pA to nA range. High resolutions can be achieved on a Cameca instrument, and on the Cameca IMS-6f the caesium beam specification is 200 nm and the oxygen beam specification less than one micron. The Cameca nanoSIMS50 instrument has a specification of 50 nm [16].

For sputter depth profiling beam currents in the nA-uA range are required and a variety of ‘gas-guns’ are available in which a gas is ionized in a plasma and the primary ions then extracted down a beam line, from the plasma source. The beams cannot usually be focused to less than a few

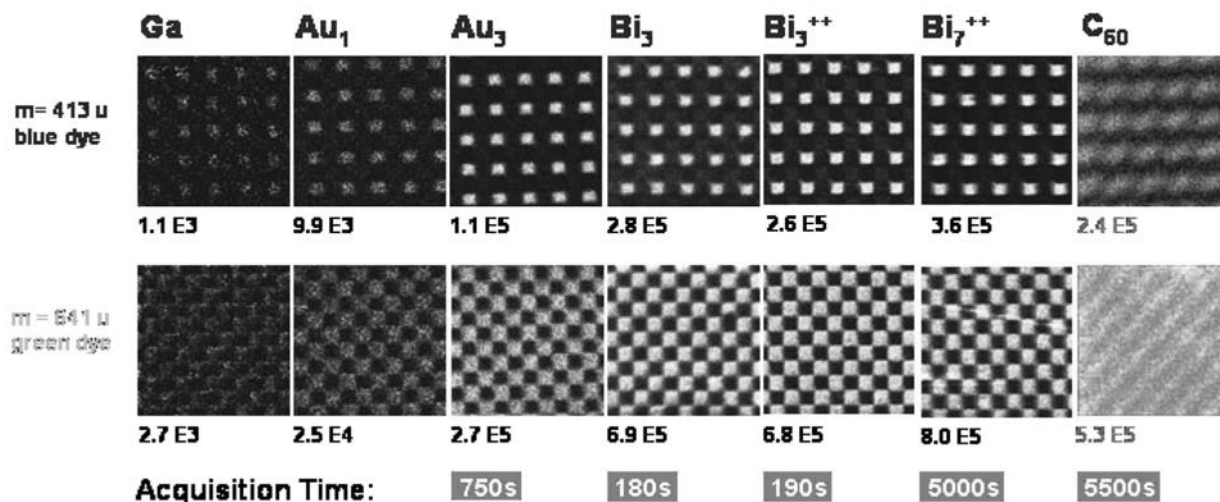

Figure 11 Efficiency of liquid metal ion sources (data from Mr. Colin Helliwell, ION TOF, www.iontof.com).

microns. Reactive ions such as oxygen and nitrogen can enhance the useful ion yield by many orders of magnitude by forming an altered layer in the near-surface which produces a favorable chemical environment for ionization. The caesium ion gun is also used for sputter depth profiling but in this case the ions are formed from a heated frit and it is difficult to achieve a beam focus better than 5 μm. A new development of major significance is the floating low energy ion gun (FLIG). This gun invented by Mark Dowsett [15] and manufactured by Ionoptika [10] can be operated with high brightness down to primary beam energies of ~250 eV with beam currents of hundreds of nanoamperes. This source has led to a new era in SIMS analysis, the era of ultra-low energy depth profiling.

The latest beam type to arrive on the market place is the IOG C_{60}^+ ion gun, manufactured by Ionoptika [5]. The C_{60} ions are produced by electron bombardment of C_{60} vapour. This ion produces high ion yields over a thousand times higher than those achieved with gallium and indium. In the example shown (Fig. 12) above a cellular structure has been imaged with indium and C_{60}^+, with the functional group of interest being over a thousand times brighter under C_{60}^+ analysis. It is not yet clear whether the high brightness of the secondary ion image is due to higher sputter rates z' or higher ionization probabilities $\alpha_{(X^+)}$ but C_{60} based sources have another very important advantage; it seems that for the first time high mass polymeric and biological molecules are being sputtered essentially intact so that analysis and depth profiling of biomaterials and polymers (see below) may be achievable.

1.3.2. Mass spectrometers

A number of different mass spectrometers are available to perform the mass filtering function in secondary ion mass spectrometry.

The cheapest and fastest of these is the *quadrupole mass spectrometer*. The quadrupole spectrometer separates ions on the basis of path stability, as they pass through an electromagnetic field established by application of dc and high frequency ac voltages to four sets of rods. For a given setting of the ac and dc potentials being applied only ions of one mass have a stable trajectory through the analyser and all others are rejected. Thus, only one secondary ion species can be mapped at a time, and if there are several elements of interest then they must be mapped in parallel. A typical quadrupole mass analyser has a mass resolution of about 300.

Mass separation can also be achieved in *magnetic sector mass spectrometers*. Magnetic sector mass spectrometers separate ions of different mass-to-charge ratio into different parabolic trajectories. By placing a series of detectors at different loci it is possible to monitor several masses simultaneously. Magnetic sector mass spectrometers and the associated ion optics have higher secondary ion transmissions than quadrupole based instruments. Mass reso-

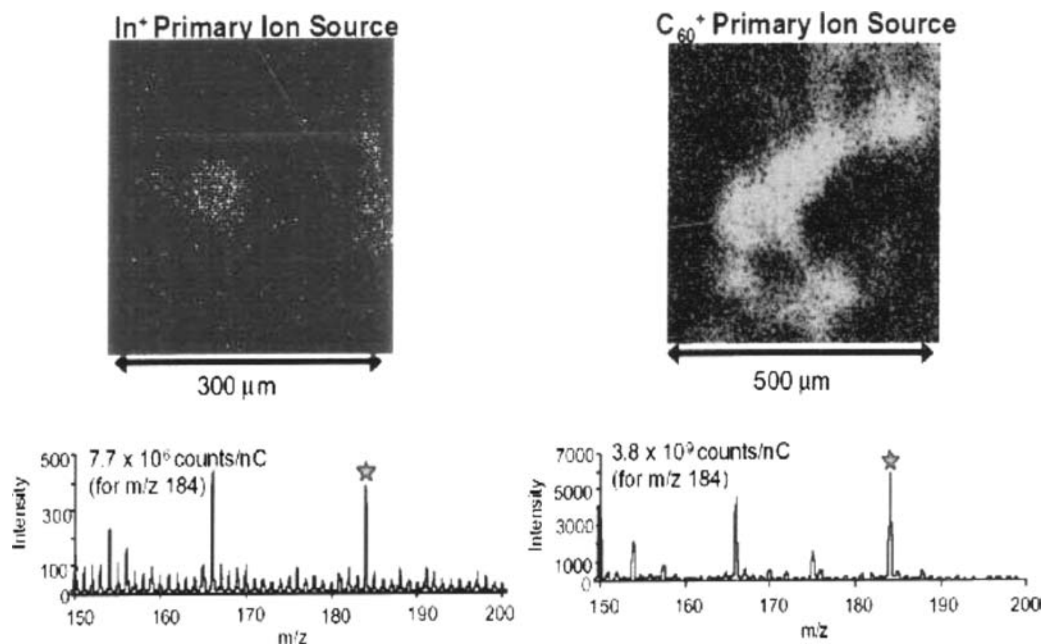

Figure 12 A cellular structure imaged with C_{60}^+ and In^+ (data from Mr. Colin Helliwell, ION TOF, www.iontof.com).

lutions greater than 10,000 can be achieved on such instruments.

A third type of analyser is based on *time-of-flight mass spectrometers*. This spectrometer must be pulsed. A bunch of secondary ions are admitted into the TOF analyser and accelerated to an energy of several keV, before being allowed to drift though a field-free region. Since all the ions have the same kinetic energy they are separated according to their speeds. As with the magnetic sector instruments, mass resolutions greater than 10,000 can be achieved. The great advantage of the TOF analyser is that no secondary ions are rejected or lost, and each data point is an entire mass spectrum. The disadvantage is that the mass analyser has to be pulsed; if the primary ion beam is 'on' throughout the analysis then a lot of information is lost, so the primary beam is usually pulsed as well. The timing associated with the operation of such an instrument can be found, for example in the ION-TOF literature [2]. In such an instrument it is possible to use the 'dead-time' for irradiation of the sample with electrons (to facilitate charge compensation) or another ion beam for sputtering.

1.3.3. Static SIMS

Static SIMS involves irradiation of the sample surface with a very low dose of primary ions. The basic premise is that during the experiment each ion arriving at the sample surface should impact on a previously undamaged site, so that the secondary ion information comes from a virgin surface. Since the lateral extent of the collision cascade from a 10 keV ion such as Ar^+ can be circumscribed within a 5 nm circle it follows that overlap can be avoided if the primary ion dose Φ is kept below a threshold of 4×10^{12} ions/cm^2 although $\Phi < 10^{13}$ ions/cm^2 is more often the figure quoted in the literature. Since the information depth in SIMS is essentially a few monolayers, this mode of analysis yields near atomic resolution on the surface monolayer. The information is usually presented in the form of mass spectra or images.

1.3.4. Imaging SIMS (lateral resolution)

In imaging SIMS the ion beam is scanned over the sample surface and maps of secondary ion images generated. It is normal to scan using a digital raster scanner with scan patterns such as 128×128, 256×256 or 1024 by 1024 being common. The relationship between pixel spacing and beam focus is a matter for attention. If the spacing is significantly greater than the beam width then a discrete series of holes will be drilled in the surface and potentially important areas left untouched.

There are two modes of imaging SIMS depending upon the mass spectrometer being used. In systems based on a quadrupole mass spectrometer, which passes only one mass at a time, only one secondary ion species can be mapped at a time, and the elements of interest must be mapped sequentially. In the Cameca nanoSIMS (http://www.cameca.fr/index.html) [16] several masses may be mapped simultaneously. In the Ion-TOF time-of-flight instrument the entire secondary ion mass spectrum is collected each time the primary ion beam addresses the sample surface.

Imaging results are in the main presented as images of secondary ion intensity across the sample surface, and

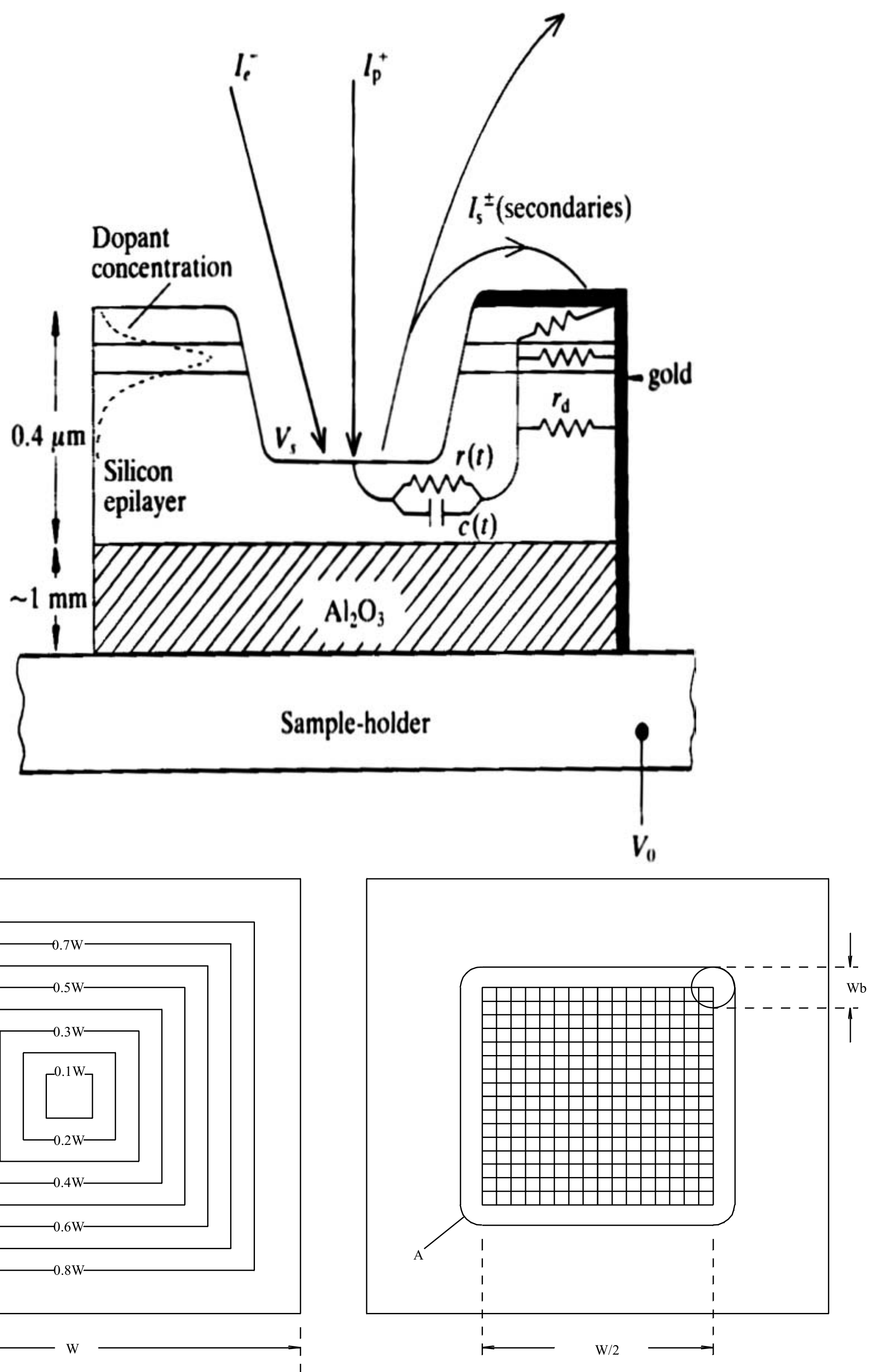

Figure 13 A schematic of a SIMS depth profile. The primary ion beam I_p^+ is scanned over the surface and a flat-bottomed crater gradually eats its way into the material. Some fraction of the sputtered flux is ionized and leaves the sample as positive/negative ions and it is these secondary ions that are useful analytically. An electron beam can be used for charge compensation, if the sample is insulating; alternatively the sample may be gold-coated. (Top) The inset shows the concept of electronic gating whereby the secondary ion counting system is only enabled when the beam is in a pre-defined area in the middle of the crater. (Bottom) Inset: Two methods of electronic gating, spiral and checkerboard. All electronic gating systems enable the secondary ion counting system only when the primary ion beam is in some defined central are of the crater, to avoid crater edge effects.

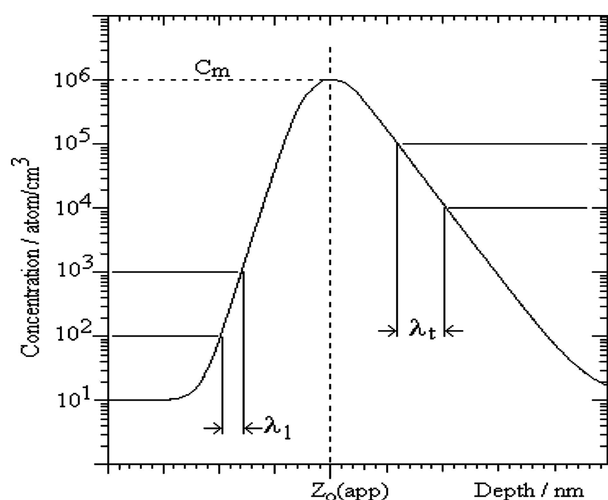

Figure 14 The depth resolution of the SIMS instrument may be assessed using a delta-doped layer. The instrumental response is a broadened peak on which the up-slope and down-slope are often linear over some depth range. λ is defined as the depth over which the signal intensity changes by a factor of ten on a linear part of the curve, and suitable subscripts are often added to denote the up-slope or the down-slope. Sub-nanometre depth resolutions can sometimes be achieved with sub-keV primary beams.

there are relatively few examples in the literature of concentration maps. The lateral resolution may be defined as the broadening of an abrupt feature introduced by the measurement process (a full-width-at-half-maximum would be a normal definition) and this broadening usually mainly reflects the beam width of the probe and the lateral cascade mixing of the probe.

1.3.5. Depth profiling SIMS (depth resolution)

The objective in a SIMS depth profile is to follow the distribution of minor and trace level elements as a function of depth. The ion beam is scanned over the surface, usually in a square digital pattern, ensuring that beam overlap exceeds 50%. Under these conditions the primary beam flux is constant over an extended area and a flat bottomed erosion pit or crater should ensure. Care is taken to ensure that the secondary ions being counted are being emitted from the flat central part of the crater, to avoid crater edge effects. Fig. 13 shows the basic idea with the beam being scanned over an extended area to ensure that a flat bottomed crater is produced. When the centre of deflection of the beam is in the central gated area all the ions being generated originate from the flat base and the secondary ion counting system is enabled. When the beam is outside this gated area secondary ions can be generated from the side wall of the crater. Some methods of charge compensation are indicated in the Fig. 13.

The raw data from a SIMS depth profile is a plot of the secondary ion intensities as a function of time and quantification involves converting this information into plots of concentration as a function of depth, by taking

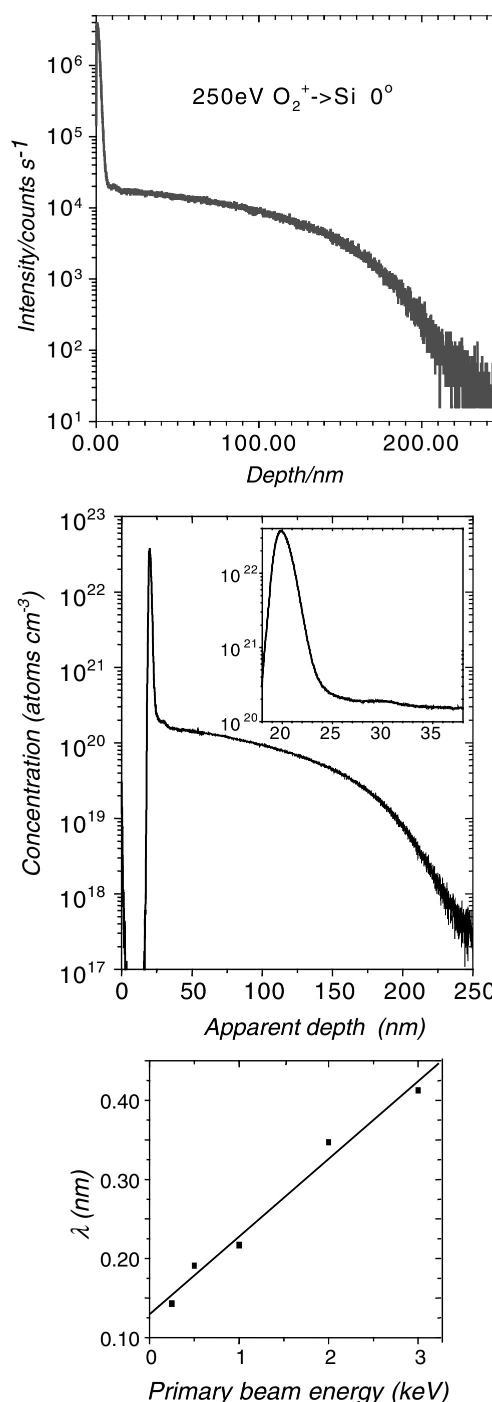

Figure 15 (a) An ultra-low energy SIMS depth profile of a 1 keV ^{11}B implant into silicon after RTP. Surface spike is a real part of the boron dose (but rises to ∼20% concentration). It is only 5 nm fwhm. The boron has precipitated to form nanoclusters of boron silicide, and a SIMS protocol was developed to quantify this. (b) The depth-profile of the boron implant, after the sample was capped with 20 nm of poly-silicon. (c) The up-slope of the boron spike above as a function of beam energy. The exponential up-slope (the depth over which the signal increase by a factor e) can be extrapolated to 0.14 nm at 0 keV (Courtesy of Professor Mark Dowsett, Department of Physics at Warwick University).

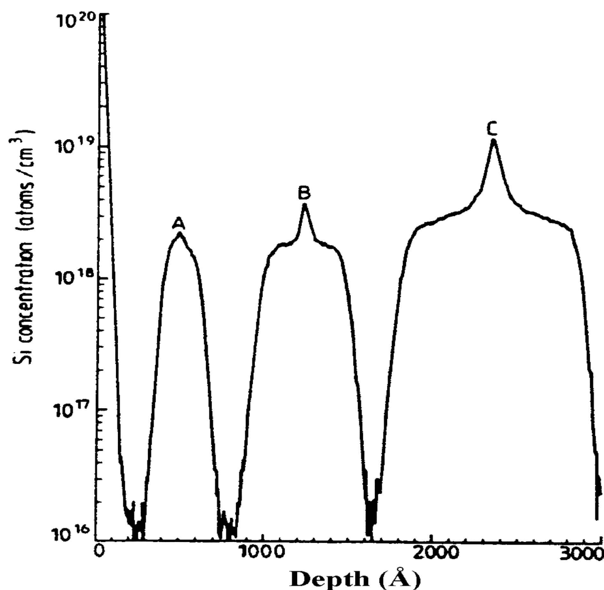

Figure 16 SIMS depth profiles of a GaAs sample incorporating three Si delta doped layers to (A) 0.4, (B) 1 and (C) 4 × 10^{13} atoms/cm^2 after annealing at 648°C for 3.5 h.

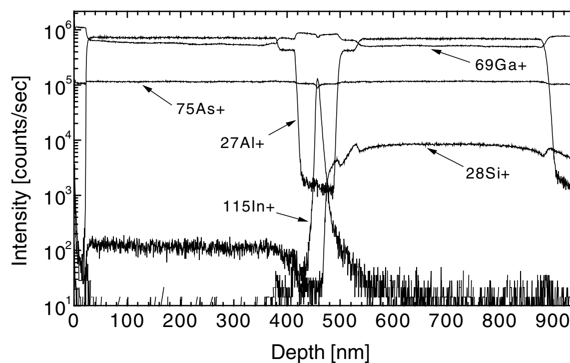

Figure 17 A SIMS depth profile though a multilayer structure together with a schematic of the intended structure. The depth profile is consistent with the nominal structure.

into account the useful ion yields of all the species of interest as well as the sputter yields of all the layers.

In SIMS depth profiling there are often two key questions;

- What is the profile shape?
- How sharply are the impurity atoms confined in the 'z' direction?

The accuracy with which a profile shape, for example a diffusion profile or an ion implant, can be measured depends upon the accuracy of the calibration procedure and on perturbations introduced by the measurement process itself. There are many different factors that lead to broadening of the true profile shape (for example uneven etching, beam induced topography, cascade induced missing processes, beam induced segregation) often referred to generically as *mixing processes* and some of these will be mentioned in the case studies. Profile broadening due to mixing processes may be measured by conducting a SIMS depth profile through an atomically abrupt 'delta' layer and measuring the shape of the signal produced. Generally the 'response function' will contain regions where the signal increases exponentially with depth (the up-slope) or falls exponentially with depth (the down-slope) and the resolution will be quoted as the depth over which the signal changes by a factor of ten (λ), with the units of nanometre (per decade change in signal intensity). An alternative is to quote the depth over which the signal changes by a factor of e. In Fig. 14 the log (Intensity) is plotted as a function of depth. At sub-keV energies one would expect sub-nanometre depth resolution.

1.4. Further information

The most important international SIMS conference takes place bi-annually and the fifteenth of these conferences, SIMS XV, took place in Manchester from September 11th–16th, 2005. The proceedings of the last four conferences are given as [17–20]. In addition to the text book by Wilson, Stevie and Magee, there are a number of other useful books including Benninghoven's book 'Secondary Ion Mass Spectrometry [21] and a book with the same title by Vickerman [22]. Vickerman has also written a more general text on Surface Analysis in which SIMS is compared to other surface analysis techniques. Static SIMS and TOF SIMS are the subject off books by Vickerman, Briggs and Henderson [23] and Vickerman and Briggs [24]. Perhaps the most useful web-site is that of the SIMS Workshop [25]. This web-site contains links to the web-sites of manufacturers, to tutorials on SIMS, and to literature.

2. Case studies in materials science

2.1. Semiconductors

The requirements of the semiconductor industry have provided the main impetus for the development of the SIMS technique. This dominance can quickly be appreciated by scanning the contents pages of the bi-annual SIMS proceedings [16–20]. Depth profiling of laterally uniform doped films to produce a plot of concentration as a function of depth was the main requirement in the eighties and nineties, and the key issue was how to optimise the depth resolution in order to keep pace

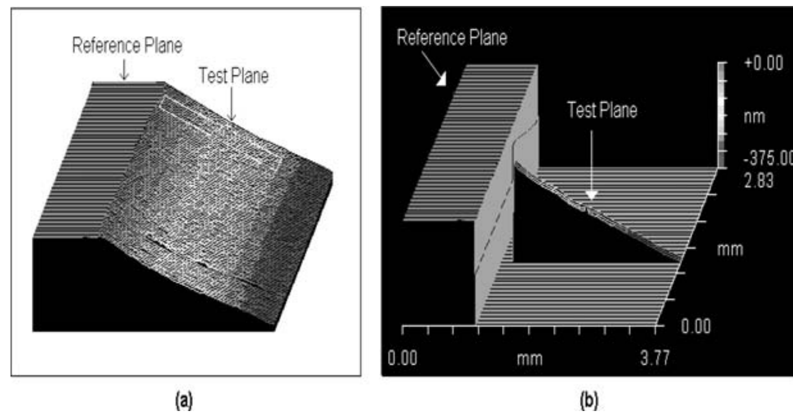

Figure 18 A ZYGO (white light interferometry) image of a bevel in silicon produced by chemical etching. The uniformity of the bevelling process is apparent [36].

with the industry requirements mapped out in the "The International Roadmap for Semiconductors" [14].

A new era in SIMS, the era of ultra-low-energy SIMS depth-profiling began in the late nineties when the floating low energy ion gun invented and developed by Dowsett [26], became a commercial reality. The FLIG gun is manufactured by Ionoptika and is now sold by Cameca on the Atomika 4500 series depth-profiling instruments [16]. Sub-keV beams and sub-nanometre depth resolution are now available to the analytical community.

Very abrupt doping structures in semiconductors such as 'delta-doped' samples present features too abrupt to be accurately resolved by SIMS depth profiling; however they are very useful to the SIMS analyst in assessing the depth resolution of the instrument.

Bellingham [27] has recently shown how ultra-shallow features in a low-energy ion implant can be resolved in a SIMS depth profile. Ultra-shallow implants are usually annealed after implantation to remove the beam induced damage and make the dopants electrically active. Sharp features in the dopant distribution often arise and these features are difficult to measure as they typically fall within the pre-equilibrium period (surface transient) in a SIMS depth profile, making quantification and dosimetry inaccurate. The sample studied was an ultra-shallow boron implant in silicon and in Fig. 15a the shape of the implant has been accurately resolved, apart from the near-surface boron spike which sits in the pre-equilibrium region of the depth-profile. The ultra low energy profile was achieved by sputtering with a 250 eV primary ion beam of O_2^+ ions at normal incidence (0°). To resolve the near-surface feature the sample surface was capped with ∼20 nm of polycrystalline silicon, and then re-analysed, thus ensuring steady state sputtering had been achieved before reaching the boron spike. The result after capping is shown in Fig. 15b. The surface spike is a real part of the boron dose (but rises to ∼20% concentration). It has a full-width-at-half-maximum of 5 nm. The boron has precipitated to form nanoclusters of boron silicide, and a SIMS protocol was developed to quantify this. The shape of the implant can be followed through five decades of concentration change (the dynamic range), and the clustering of dopant atoms near the peak of the implant is clearly visible. The profile shape is believed to be accurate to ±1 nm, and this precision is termed the 'depth resolution' (formal definitions follow). Clearly this type of analysis provides vital information for the semiconductor scientist. Analysis of the capped sample at several energies (Fig. 15c) revealed that the up-slope on the boron spike λ_u was very sharp. This resolution parameter was plotted as a function of beam energy and extrapolated to a 'zero-energy' slope of 0.13 nm, a limit which the authors suggest is due to topography (presumably together with the information depth of the technique). This example illustrates that features normally too close to the surface to be resolved may be measured accurately, if the sample is first capped. The measurement also indicates the sort of depth resolution that can be achieved with state-of-the-art instrumentation.

It is not always necessary to use state-of-the-art depth resolution to measure important phenomena. Beall *et al.* [28] used SIMS and Capacitance-Voltage (CV) depth profiling to measure delta layer broadening due to post-growth annealing. Delta layers of a few areal densities were studied (0.4×10^{13}, 1×10^{13} and 4×10^{13} atoms/cm^2) by SIMS (Fig. 16) and it was found that for short anneal times the profiles broadened at a rate that increased with increasing areal density. For long anneals, e.g. 3.5 h at 648°C, the lightly doped layers spread into an approximately Gaussian peak, which was as expected. For the high dose peak, the shoulder is nearly 100 nm wide. Beyer *et al.* have used SIMS depth profiling to determine small amounts of inter-diffusion at the interface between aluminium arsenide and gallium arsenide layers in a multi-layer distributed Bragg reflector

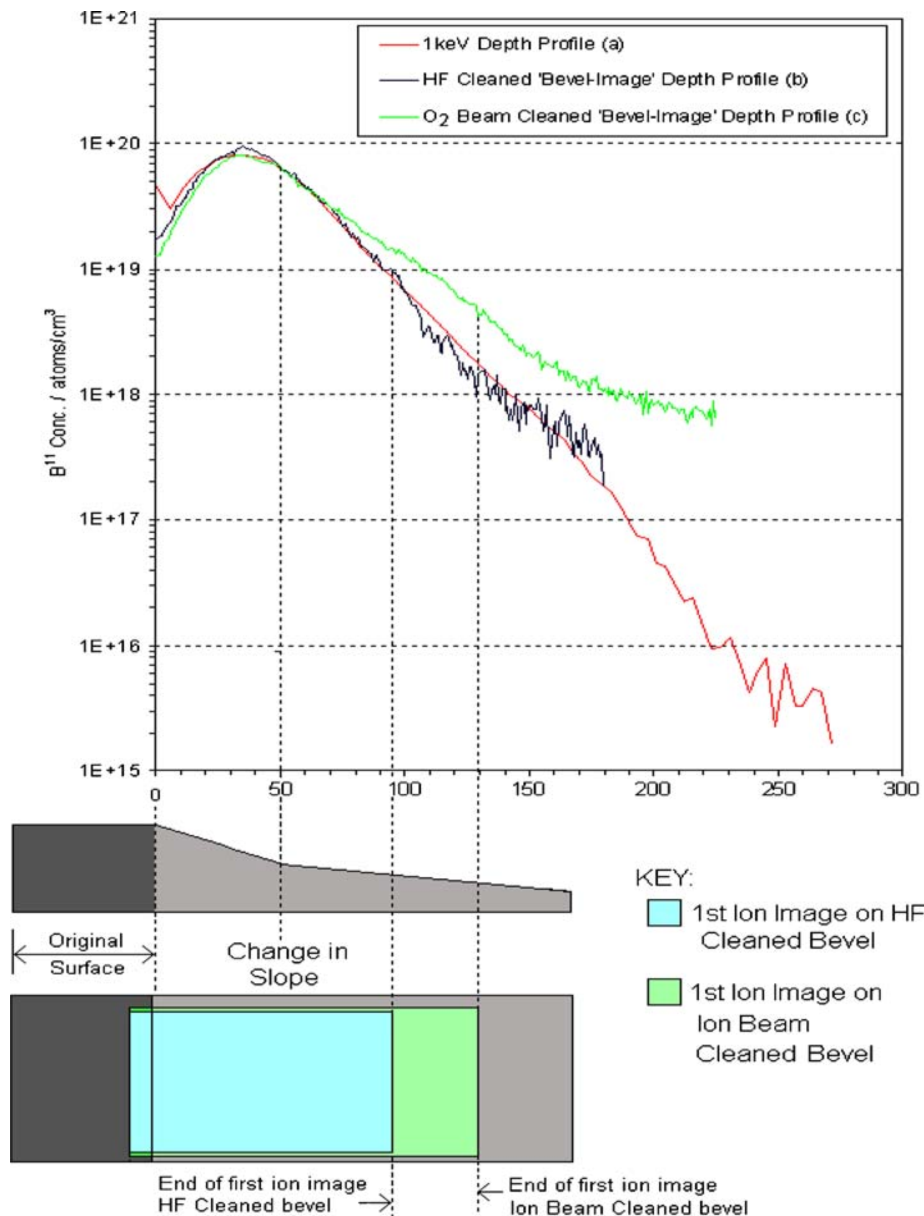

Figure 19 A 'depth-profile' of a shallow boron implant in silicon. A 1 keV SIMS depth profile with an oxygen primary ion beam is compared with a linescan analysis down a bevel. The bevel has been cleaned with hydrofluoric acid prior to SIMS analysis (blue curve) and this is more effective than ion beam polishing (green curve).

[29, 30]. Diffusion lengths of less than 1.1 nm were determined for aluminium diffusion in gallium arsenide, corresponding to a diffusion coefficient of 10^{-17} cm^2/s.

SIMS depth profiling has been very successfully applied to the analysis of multi-layer structures. For a fully quantitative analysis it is necessary to measure the sputter yields of all the layers and to know the useful ion yields for all the dopant-matrix compositions of interest. An example is a depth profile of a laser structure grown by MOCVD at University of Leipzig in Germany shown in Fig. 17. The structure was analyzed to a depth of more than 900 nm. The active region consisted of an $In_{0.15}Ga_{0.85}As$ layer 10 nm thick embedded in the GaAs quantum well (35 nm from each side). All this is sandwiched between Al_xGa_{1-x} As barriers of graded composition ($x = 0.2$ and 0.35) and Zinc and Si are present as dopants. The cross section of the structure together with layer thicknesses and composition is shown in the figure, above the plotted depth profile. The SIMS analysis, after depth calibration, is used to validate the structure, and to check the uniformity of the doping. It should be emphasised that the outcome of this analysis is not fully quantified, for example no account has been taken of the different sputter rates of the different layers or of the variations in ion yield of the dopants from layer to layer. Nevertheless it is clear, without the need for full quantification that the structure is essentially as specified,

but that that the doping level is not completely constant throughout the film.

Sometimes alternative analysis strategies are useful, for example reverse side SIMS analysis [31, 32] where SIMS induced artifacts can be moderated by analysing from the back surface to the front. Another approach of interest is the analysis of shallow bevels into the structure of interest. Hsu [33, 34] and Fearn [35, 36] have developed a method of chemical bevelling of III–V materials and silicon, respectively, that involve gradually immersing or removing a sample in an appropriate etching solution. Features thinner than the depth resolution of the technique can be magnified into features broader than the lateral resolution and bevel magnifications in the range 1,000–10,000 can be produced. The bevel shape can be assessed using a Zygo white light interferometer and the uniformity that can be achieved is highlighted in Fig. 18. Subsequent analysis involves SIMS imaging or line scanning along the bevel plane. One of the advantages of the beveling procedure is that the depth of origin of the secondary ions can be determined retrospectively, from the position of the crater formed during imaging or linescan analysis. The success of this technique can be gauged from Fig. 19, where a shallow boron implant in silicon has been measured over three orders of magnitude of concentration.

Hsu [34] has analysed aluminium deltas in gallium arsenide and was able to produce a very high depth resolution on both the leading edge and trailing edge of the deltas. The bevel was produced using a $NH_4OH/H_2O_2/H_2O$ solution. Fig. 20 shows the results. An up-slope of 0.9 nm/decade and a down-slop of 0.6 nm/decade were produced (these are very high depth resolutions and using the exponential up-slope and down-slope definition correspond to 0.36 nm and 0.26 nm, respectively).

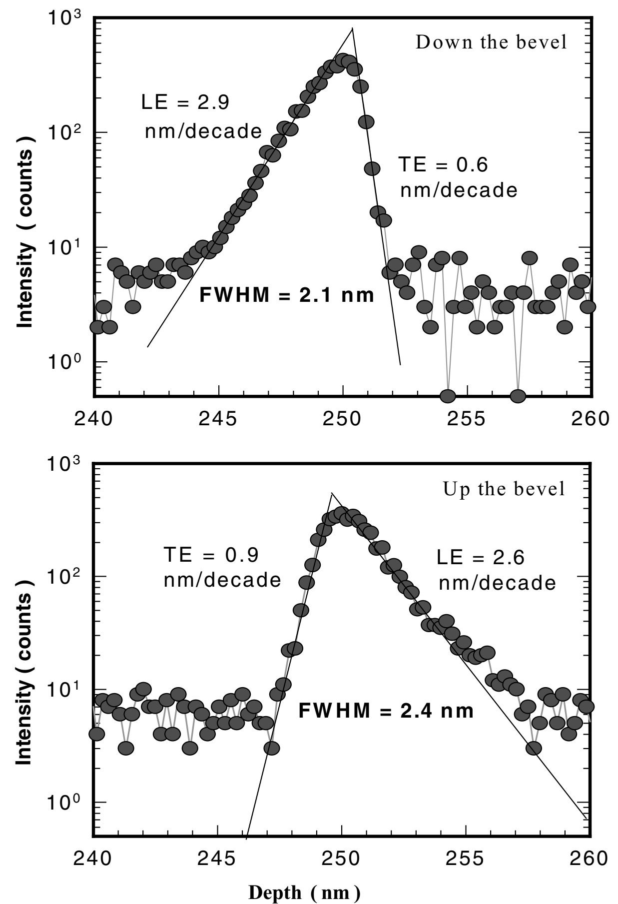

Figure 20 The depth calibrated linescan profile of an Al δ-doped layer (1 ML). The sample was chemically bevelled with 1:1:600 $NH_4OH/H_2O_2/H_2O$ solution and has a bevel magnification of about 8.3 $\times$ 10^3. Both the upward linescanning and the downward linescanning are presented.

2.2. Superconductors

Montgomery has shown how SIMS depth profiling and focused ion beam imaging may be used to validate superconducting test structures and to determine inter-diffusion between the layers in a multilayer structure. He used atomic force microscopy to assess the surface and beam induced topography, which were the factors limiting the ultimate resolution that could be attained [37]. Results of a depth profile of an YBCO/SrTiO3/MgO/YIG multi-layer are shown in Fig. 21. The analysis was achieved using a 15 keV oxygen primary ion beam and the layer thicknesses corrected for their different sputter rates (which were measured in separate experiments). Montgomery also developed techniques for imaging the structure, using the FIB system, and then reconstructing a ‘pseudo depth profile’ from the image data. This is an interesting and important approach when the sample is very rough.

2.3. Glass

SIMS depth profiling can be used to study slow processes at the surface of a material and SIMS imaging can be used to analyse particulates and contaminants on the surface. The advent of ultra-low energy depth profiling means that these processes may be monitored in real time without the need for accelerated ageing. For example, a corrosion rate of 1 nm per day corresponds to 0.365 millimetres per millennium, and it is now practicable to construct SIMS-based experiments to monitor the early stages of corrosion, oxidation or diffusion processes with these kinetics.

Glass is being considered as a containment material for radioactive waste [38, 39] but it is important to recognize that there is nothing inherent in the glassy state that implies stability, and the relative stability of a glass depends upon its composition and the environment. Recently [40–42] for example we have been studying the corrosion of vessel glass from the collection at the V&A museum as well as the pitting corrosion often observed on contemporary float glass.

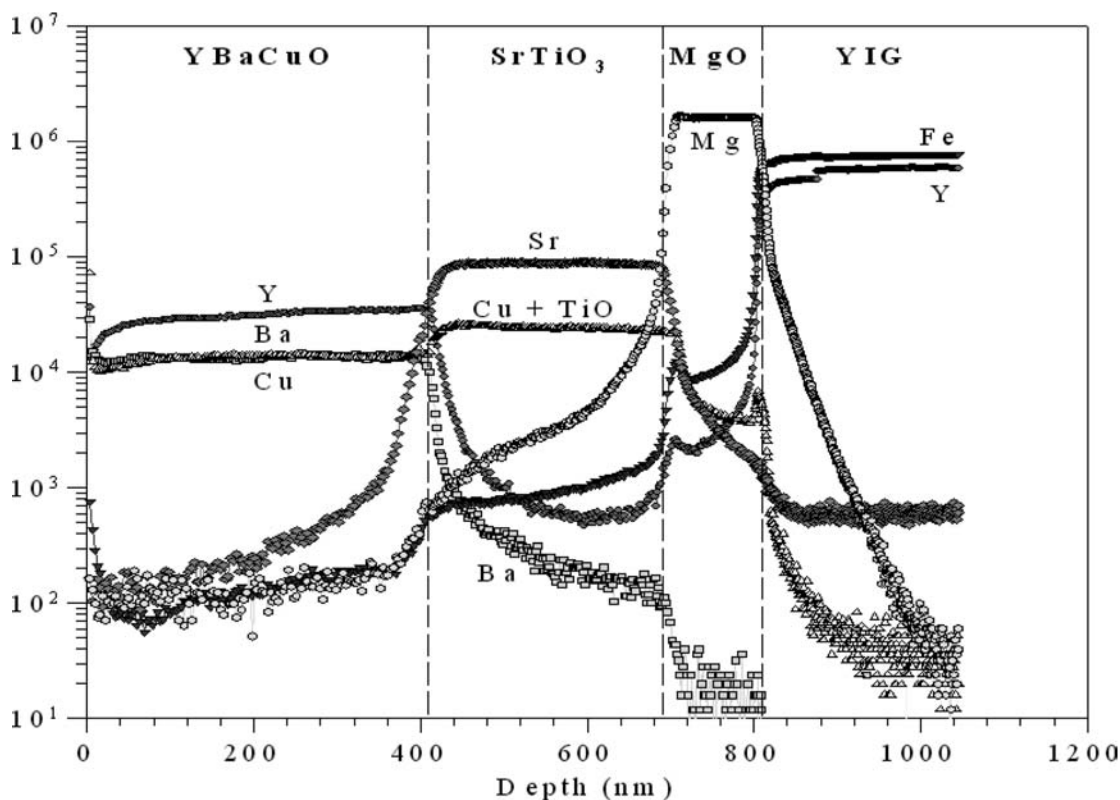

Figure 21 A SIMS depth profile of a superconducting multi-layer structure showing the resolution of the individual layers and some inter-diffusion between the layers.

A survey of the collection at the Victoria and Albert Museum (V&A) has indicated that 25% of the total glass collection is particularly vulnerable to glass corrosion and shows some sign of deterioration [43]. An example of a Venetian goblet that has undergone significant corrosion is shown in Fig. 22. A stability diagram may be constructed to represent the relative stability of such glasses and such a diagram in shown in Fig. 23. We have conducted experiments on analogue glass of the same composition, to determine the best conditions of active and passive conservation of the glass. The composition used is shown in Table II.

The corrosion of low-lime glass involves an ion-exchange process with sodium and potassium ions moving to the surface of the material, being replaced by hydrogen ions from the moisture in the atmosphere [44]. Thus the surface region becomes depleted in alkali and gradually forms a gel-type layer. The alkali ions react with gaseous species to forms salts such as carbonates on the surface of the glass, and the surface gradually roughens. The presence of these surface salt particles must be considered when interpreting the SIMS data. The development of surface topography as the corrosion process proceeds is shown in Fig. 24. The salt deposits have been analysed by FIB and SEM Energy Dispersive X-ray Analysis (EDX). Local area FIB-SIMS analysis of a particle is compared with a clear area of the surface in Fig. 25. It is clear that the particles are soda rich and further work confirmed they were mainly sodium carbonate. These salts have to be removed before a SIMS depth profile to avoid uneven etching, since the depth resolution is often severely compromised in the analysis of such materials and can never be better than the topography in the etch pit [45]; the salts should also be removed to avoid mass interferences (for example at mass 28 due to CO).

A typical SIMS depth profile of such a glass is shown in Fig. 26. Secondary ion intensities are plotted as a function of depth, using a linear intensity scale, and assuming no changes in sputter rate with depth. The analysis of glass and other insulating materials present extra challenges to the analyst due to the possibility of changes in the electric potential on the crater base as the analysis proceeds due to the build up of electrical charge from the primary ion beam. This in turn changes the secondary ion extraction field between the sample and the secondary ion analyser leading to spurious changes in signal intensity. In these analyses we used a coincident electron beam to avoid this problem.

It is important to recognize that there are a number of caveats that must be remembered when interpreting this data. Firstly the relative intensities of the ions do not reflect the relative concentrations, since different species have different ionization probabilities α. Secondly the

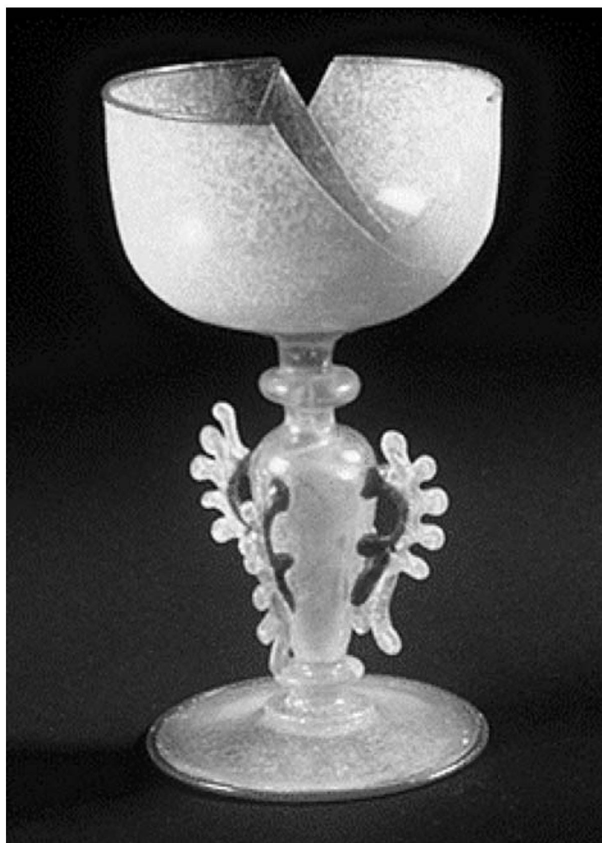

Figure 22 The effects of atmospheric attack on a 17th Venetian Goblet. The glass is low in lime and vulnerable to attack by atmospheric moisture.

system is not in the 'dilute regime' so there may be subtle changes to α for each element, as a function of composition, which would need to be determined to calibrate the concentration axis. Finally there is a large change in composition from the surface to the bulk, and changes in sputter rate are probable, and would have to be accounted for to make the depth scale totally accurate, however in practice we have determined these changes in sputter-rate to be a few per cent at most. The analysis yields a good representation of the changes in surface chemistry as a function of depth.

The key indicator of the rate of corrosion in these glasses is the sodium profile. The progressive leaching of sodium in this system as a function of time (0, 48, 72, and 96 h) is shown in Fig. 27. The intensities have been converted into concentrations using the bulk concentration of sodium as the standard and assuming no significant change in α with concentration. It is clear that the thickness of the silica gel type surface layer τ(Na) increases with ageing time. The number of sodium atoms leached out of the glass is represented by the 'missing' sodium atoms φ(Na), as indicated in the inset to Fig. 27. This parameter φ(Na) may be preferred over the thickness τ(Na) in assessing the extent of the corrosion process.

2.4. Stainless steel

In many areas of materials science it is important to assess the effect of inclusions / particulates on the local surface chemistry. One example is so-called 'stainless steel' which can be susceptible to pitting corrosion (localised dissolution). In a recent study the chemistry in the region around some manganese sulphide inclusions in a 316 stainless steel (17.65% Cr) was assessed using FIB SIMS [46]. Initial experiments were conducted using a FIB SIMS linescan with the primary beam (30 keV gallium) focused to ~100 nm, but the secondary ion signal intensities were too low so the analytical volume was increased by using annular rings for each data point as shown in Fig. 28. The secondary ion intensities of Cr^+ and Fe^+ were recorded for each position and the ratio plotted as a function of distance from the inclusion. Fig. 29 shows that the area around the MnS is depleted in chromium by over 50% and is vulnerable to attack.

Understanding the chemical make-up of the thin oxide film that passivates reactive metals such as titanium, aluminium, Fe-Cr alloys and stainless steel is of vital importance since it is these films that impart the corrosion resistance to the material. This film is often only a few nanometres thick but with the advent of ule-SIMS depth profiling it is now possible to determine the internal structure of the oxide with sub-nanometre depth resolution. Fe-Cr alloys with greater than ~13% Cr are spontaneously passive and are termed stainless steels. There is no consensus on the mechanism of passivity or the chemistry and structure of these passive films so ultra-low-energy (ule)-depth profiling was used to look at the effect of alloying additions on air-formed thin oxide films on Fe-Cr alloys and 304 stainless steel (Fe-18Cr-8Ni) [47]. Analyses were conducted with 25 nA of 500 eV Cs^+ incident at 70° to the surface normal scanning over a 600 μm square (the craters are elongated in one direction). In this case the secondary ions monitored were FeO^- and CrO^-.

Analysis of samples with compositions above and below the critical composition at which the material becomes stainless (a 17.4% compositional threshold is predicted by the percolation theory of passivity developed by Keddam and then by Sieradzki and Newman [48]) revealed significant changes in the shape of the iron and chromium mass channels with composition as shown in Fig. 30. In all cases the FeO^- peaks were found to be closer to the surface than the CrO^- peaks indicating a distinct separation between the Fe and Cr surface oxides.

2.5. Micrometeoroids

An increasingly important role for SIMS is the characterization of small particles; these may for example be pollutants in the atmosphere, contaminants on semiconducting wafers or even micrometeoroids. Recently

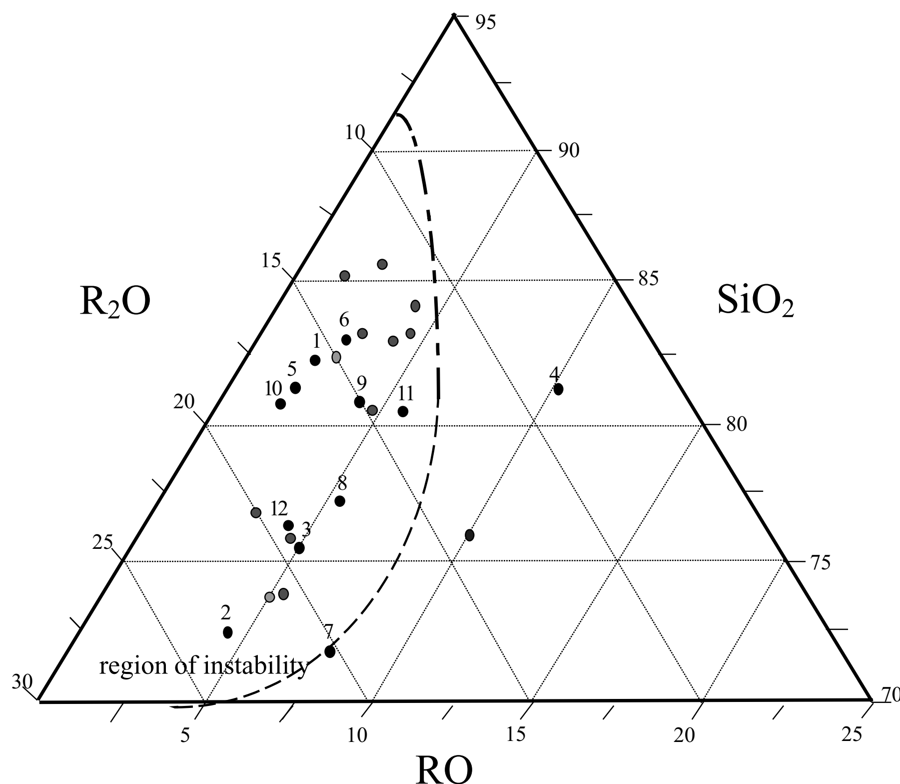

Figure 23 A stability diagram for glass with the three axes representing network former, flux and stabiliser. Triangular representation of the chemical compositions of various crizzled glasses. (The region of instability due to the lack of stabilising oxides lies to the left of the dashed line). • Modern soda lime silica glass.

micrometeoroid impacts have been studied using focused ion beam (FIB) SIMS [49–52]. Samples of solar cells from the Hubble Space telescope were assessed and a small micrometeoroid identified in a large area FIB SEM scan. The FIB was used to produce a 'double' cross-section through the particle (Fig. 31) which was then imaged at two different angles. Mass spectra revealed that the sample was a FeNi micrometeoroid and the FIB SEM images revealed the internal grain structure, through channeling contrast. The FIB is also being used to prepare TEM cross-sections into impact sites. Finally FIB is considered as a sample processing tool for the Stardust mission. In this mission aerogel, an ultra-low density glass, is being used to capture micrometeoroids. The FIB is being used to mill away the aerogel around an impact track so that the remnants of the particle can be revealed for in-situ analysis, for example by SEM or SIMS [51, 52].

2.6. Solid oxide fuel cells

Solid oxide fuel cells (SOFC) are an increasingly important new source of clean energy and are impacting on two key technological areas, namely energy and transportation. At the heart of the SOFC is an electrochemical cell with anode, cathode and electrolyte based on polycrystalline oxide ceramics and cermets. The ionic transport of oxygen ions and protons through these materials is a key aspect of the performance of these devices. Measurement of oxygen ion transport through an oxide ceramic is directly measured in the bulk material by the use of the stable oxygen isotope ^{18}O [53]. In the so-called 'isotope exchange/diffusion profile technique' SIMS is then used to measure the ^{18}O and ^{16}O depth profiles. Often the diffusion lengths are rather too long for a conventional SIMS depth profile (>10 μm) and so the ceramic pellet is mechanically cross-sectioned and the ion beam scanned over the area of interest (Fig. 32). The scan length of the Atom-

TABLE II The target composition (from a low lime Venetian goblet) and the actual composition of the replica glass

Oxide	SiO_2	Na_2O	CaO	MgO	K_2O	Al_2O_3	Fe_2O_3	MnO
Ideal Wt% of Oxide	70.60	20.25	2.61	1.07	3.68	1.10	0.31	0.37
Actual Wt% of Oxide	72.67	17.66	2.74	0.74	3.25	1.21	0.24	0.36

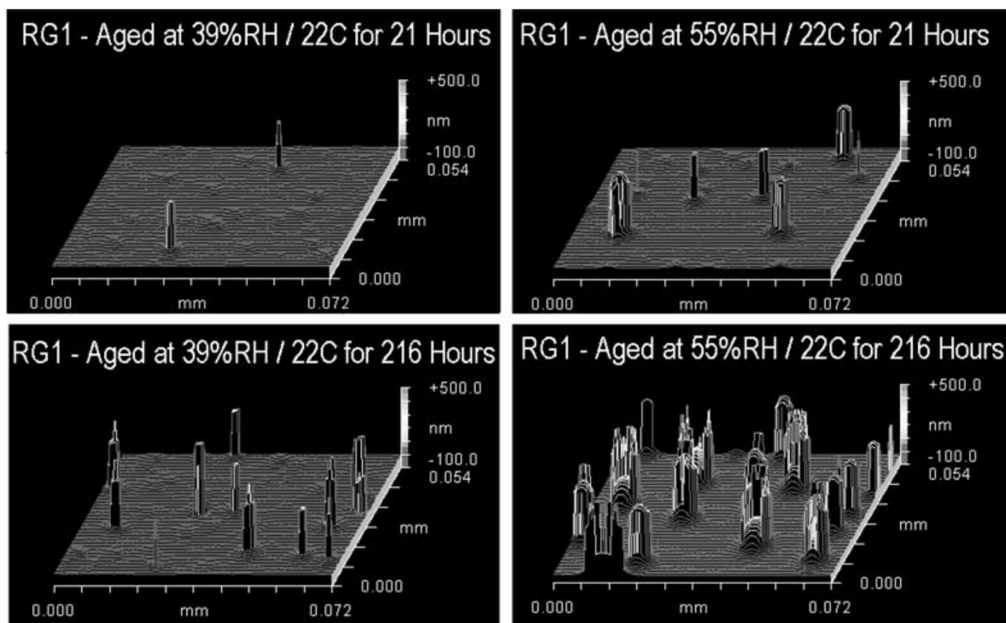

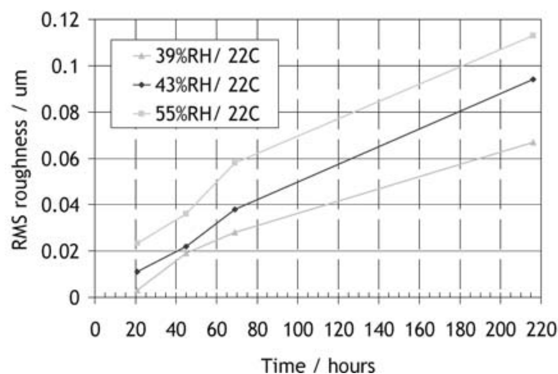

Figure 24 The development of surface topography on the surface of a low-lime glass (RG1) as a function of humidity and time. The topography will compromise the depth resolution in any subsequent SIMS depth-profile analysis and the salt may introduce mass interferences into the analysis.

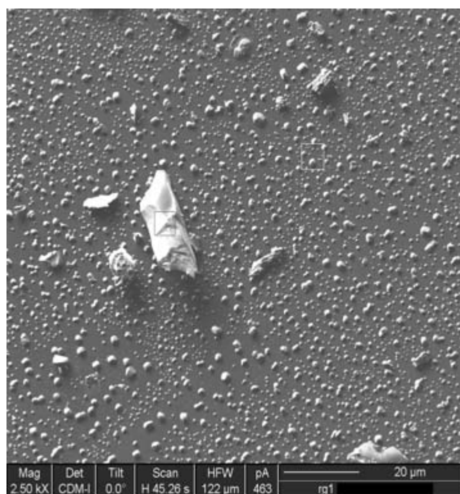

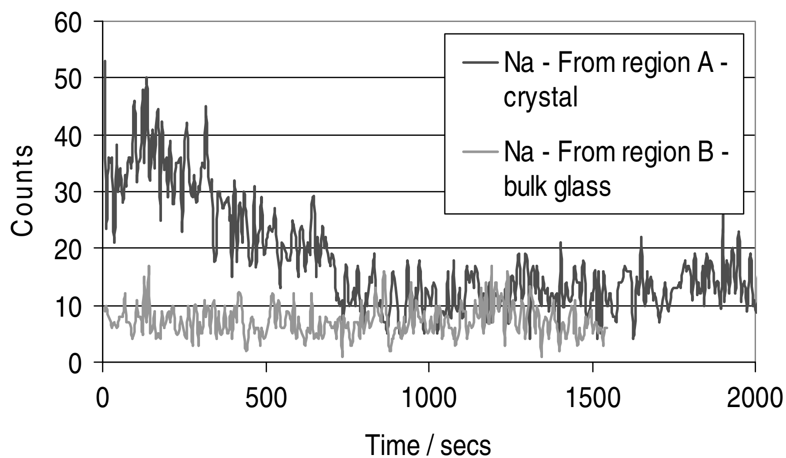

Figure 25 Salt deposits accumulating on the surface imaged in the FIB in the SEM mode. Two areas were analysed for sodium.

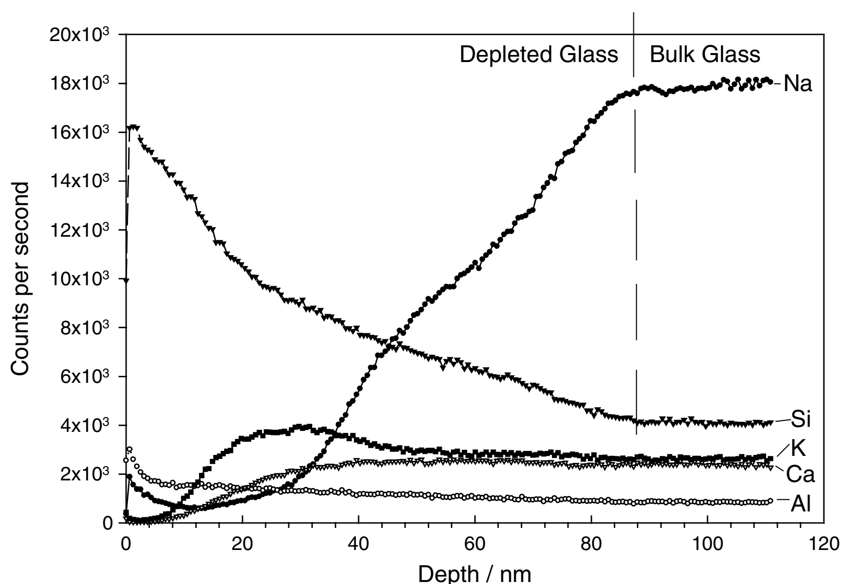

Figure 26 A typical SIMS depth profile of glass RG1 aged at 55%RH and room temperature for 96 h. A linear scale is used for the secondary ion intensities, and the depth scale has been calibrated by assuming a uniform sputter rate throughout the analysis.

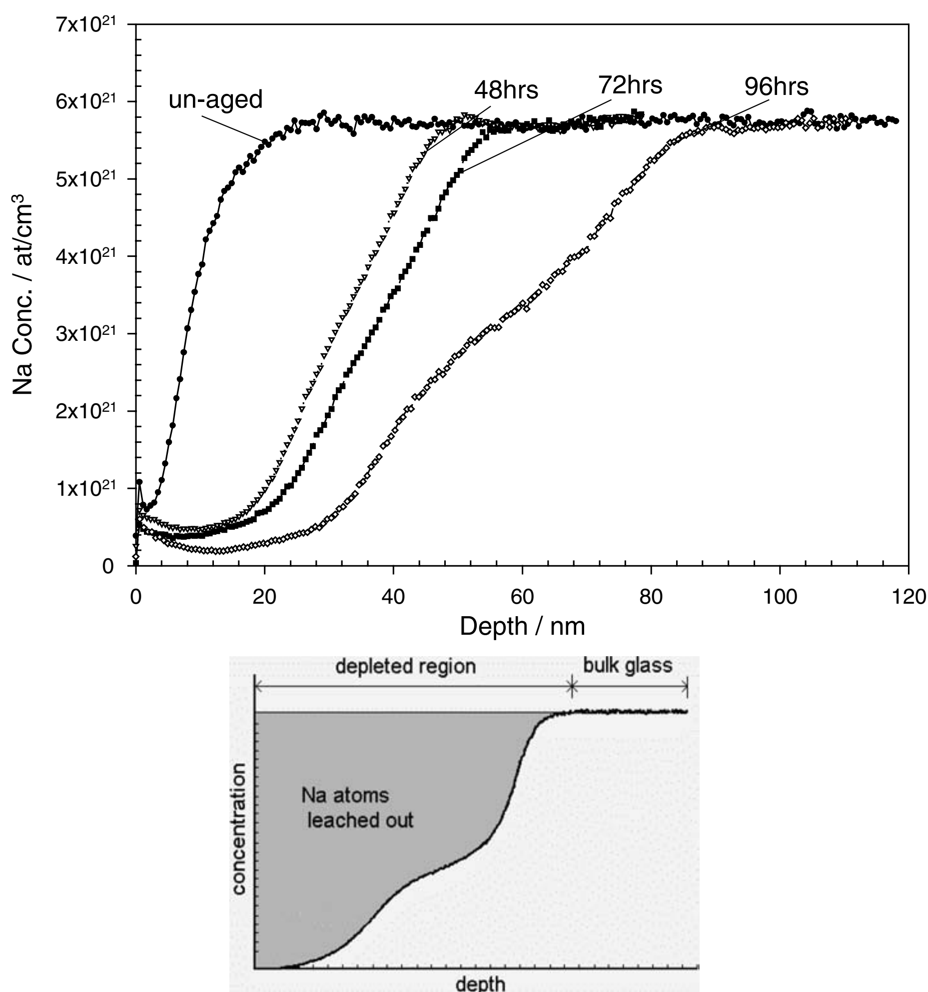

Figure 27 The Na profiles for samples aged at 55%RH and room temperature for 48, 72, and 96 h, compared to the un-aged glass. Inset: Schematic showing the area representing the leached sodium atoms on the SIMS concentration-depth profile.

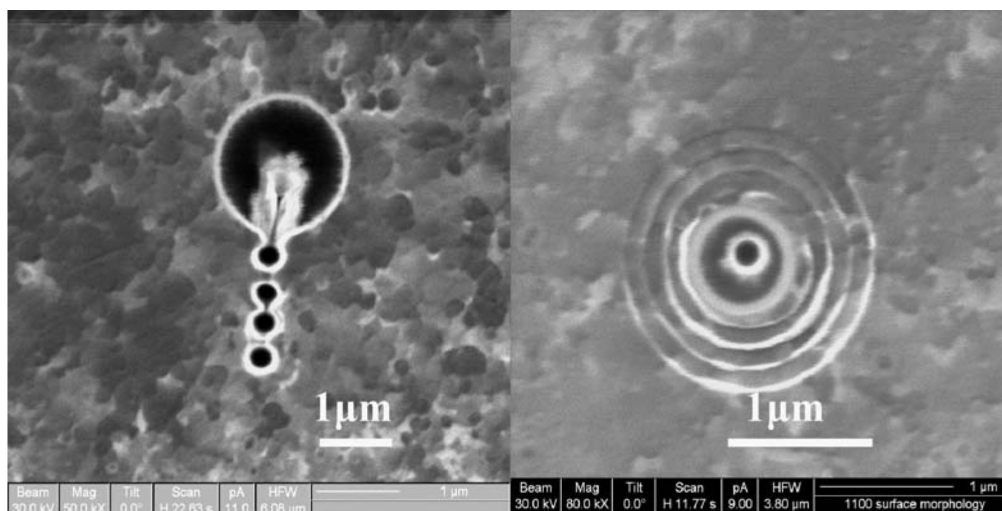

Figure 28 (a) FIB SEM image of an area analysed by a SIMS linescan. The region close to a manganese sulphide inclusion in 316 stainless steel has been investigated. The individual pixel positions generated in the linescan analysis are clearly revealed. Unfortunately the analytical volume is too low in this mode of analysis to achieve the required sensitivity to chromium and iron, so a series of annular rings were used instead (see (b)). (b) FIB SEM image of the region around a MnS sulphide inclusion after SIMS analysis. A series of annular rings were used for the SIMS analysis to improve the analytical volume per data point.

ika 6500 used in these experiments was 2 mm (2000 μm). The use of a stable isotope in a diffusion experiment is an approach that is clearly transferable to other systems. By analysing cross-sections the effective 'depth-of-analysis' in the SIMS depth profiling instrument is increased from 10 to 2000 μm. A typical result is presented in Fig. 33. If the SIMS depth profile is required in site-specific locations, then FIB ion beams are ideal for both sectioning by ion erosion and for oxygen isotopic profiling.

2.7. Conservation science

Conservation science is concerned with the search for methods of passive and active conservation of museum objects. Passive conservation relates to the conditions of storage such as temperature and humidity as well as conditions of illumination. Active conservation relates to treatments which can slow down or arrest the processes of deterioration. Surface analysis of museum objects presents some special challenges because the provenance of the raw materials may not be known and the raw materials are often 'natural' multi-component ingredients such as clay, plant ash, quartz and so on. Furthermore there is often uncertainty about the processing conditions and the environmental history under which the objects have been stored. Whilst the objects have been in the museum there may well have been previous conservation treatments that may be poorly understood and undocumented. Generally the surfaces are rough and they may often be porous.

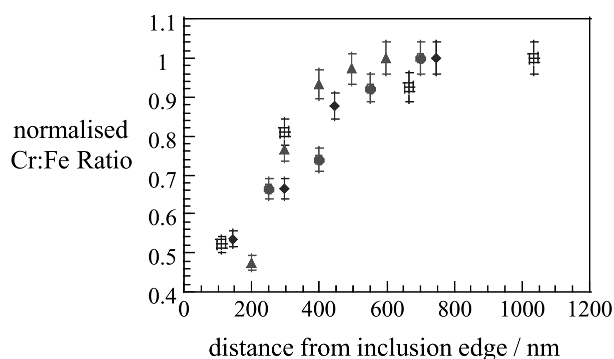

Figure 29 The ratio of secondary ion intensities of Cr / Fe as a function of distance from the centre of the MnS inclusion. The ratio has been normalised (set equal to unity) for the bulk. The chromium is depleted by over 50% close to the inclusion. 100 nA 30 keV Ga^+ ions (beam width ~100 nm).

In addition to these challenges the research should be compatible with the ethics of conservation which state that all treatment should be adequately documented, structural and decorative falsification should be avoided, it should be possible to return the artefact to its original condition even after long periods of time, (the principle of reversibility of process) and the sampling should be non-destructive. Also so far as is possible decayed parts of an object should be conserved and not replaced and the consequences of ageing should not be disguised or removed. Dowsett and Adrieans have written an important review in this area '*The Role of SIMS in Cultural Heritage Studies*' [45].

Recently SIMS has been applied to a variety of areas including laser cleaning, the tarnishing of silver in museum cabinets [54] and vessel glass corrosion [40–45]. The work on laser cleaning is based on the hypothesis that the high sensitivity of SIMS allows us to monitor changes to the surface chemistry during laser cleaning, long before they become visible to the human eye, as can

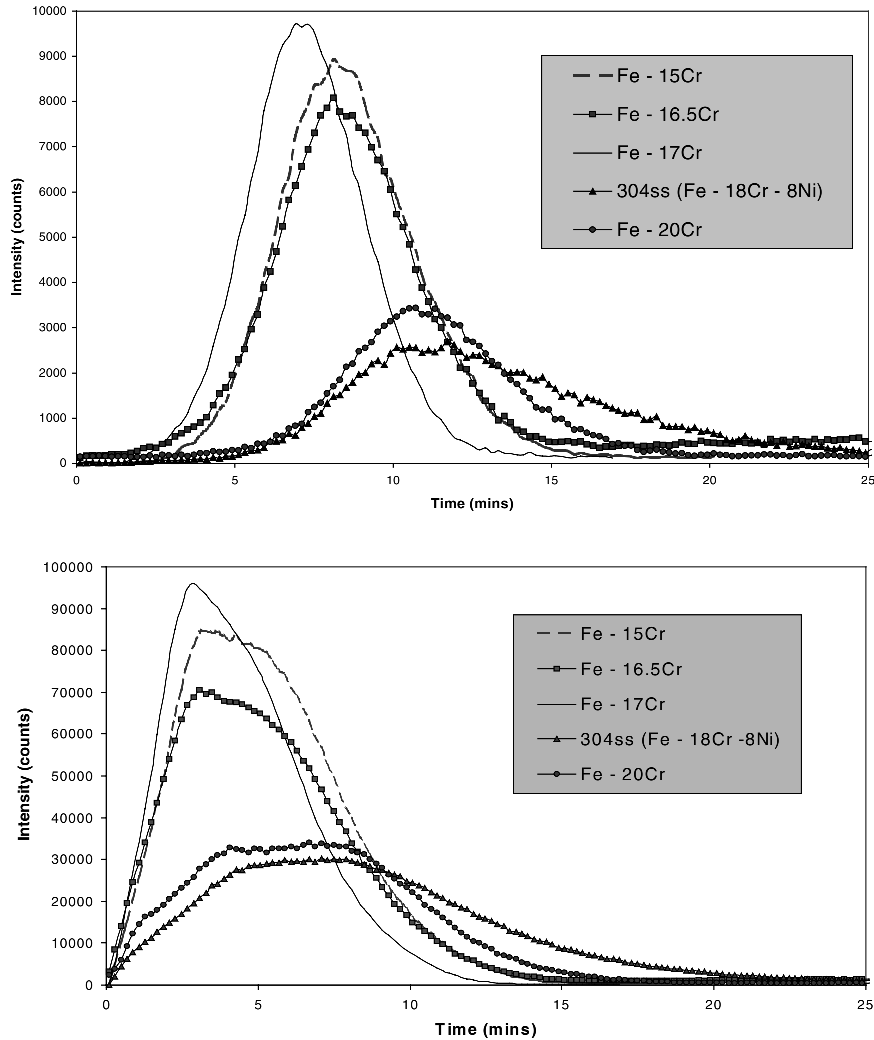

Figure 30 Depth profiles of the oxides of five steel samples containing different levels of chromium. The upper figure shows the depth-distribution of chromium (monitored as the CrO^- ion), the lower figure shows the depth-distribution of iron (monitored as the FeO^- ion). Cs^+ primary beam, 500 eV, 26 nA. Crater size of 600 μm.

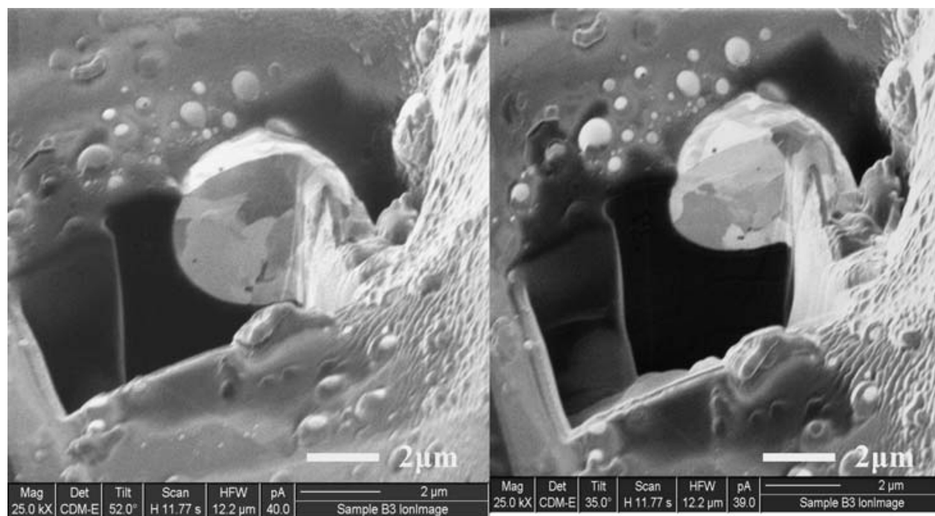

Figure 31 FIB SEM images of a micrometeoroid previously milled to create a 'double-cross section'. The images are taken with the sample stage rotated to 35 and 50 degrees respectively and the channeling contrast clearly reveals the grain structure.

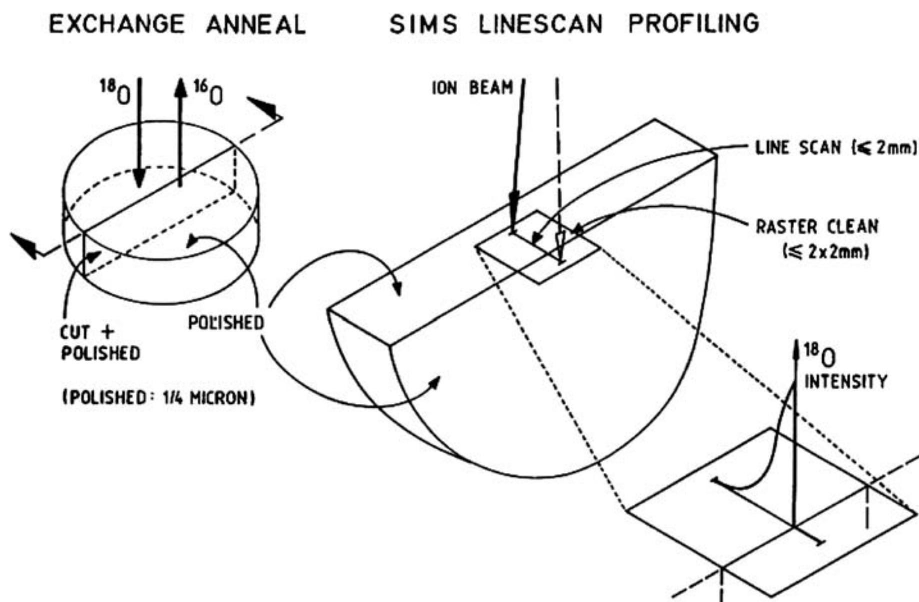

Figure 32 The experimental procedure involved in stable isotope analysis of a cross-section in the SIMS instrument.

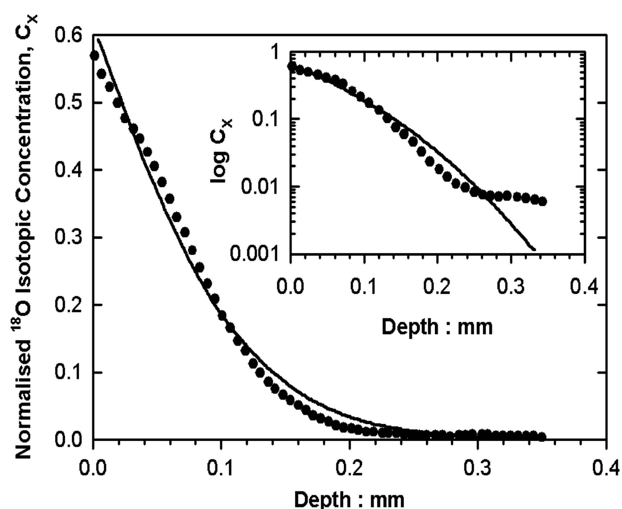

Figure 33 The ^{18}O isotopic ratio depth profile and fitted solution to the diffusion equation for the cobalite perovskite $(La_{0.6}Ca_{0.4})(Fe_{0.2}Co_{0.8})O_{(3-\delta)}$. Note that the depth axis in centimetres.

re-contamination of the surface after laser cleaning [55]. The laser used in this work has been supplied by Lynton Lasers [56] and is a dual beam Nd YAG pulsed laser. It is shared by the members of the London laser Consortium, a partnership between Imperial College, The Natural History Museum, the Victoria and Albert Museum, the City and Guilds College and the Royal College of Art.

Laser cleaning is most effective when there is strong absorption of the laser radiation by the 'dirt' and very little absorption by the underlying surface to be preserved. A good example of this was the cleaning of an 18th century ladies riding costume from the collection at the V&A museum [57]. Some threads were removed for analysis and the static SIMS spectrum from the Millbrook mini-SIMS (Fig. 34) suggested that the contamination was primarily due to handling contaminants (salts of sodium and potassium) and hydrocarbons. After laser cleaning the ratio of these peaks to the silver peak all fell considerably indicating the effectiveness of the laser cleaning process. The significance of this result is that conventional wet cleaning approaches cannot be used on this garment, as they will destroy the silk thread that the silver is wrapped around.

Whilst it is true that SIMS relies upon the removal of atoms to generate an analytical signal, the areas analysed are extremely small and the number of atoms needed can be a fraction of a monolayer so that the impact of the analysis cannot generally be seen with the naked eye.

2.8. Aerospace alloys

The mechanisms and kinetics of oxidation of aerospace alloys are of critical importance for components such as turbine blades. Stable isotope exchange SIMS depth profiling experiments using labeled oxygen have been used by Garriga-Majo [58] and Alibhai [59, 60] to gain insights into these processes.

In [59] above Alibhai investigated the oxidation resistance properties of platinum aluminide coatings on nickel based super-alloys. Samples received a two stage sequential oxidation in oxygen 16 and then oxygen 18 enriched gases at 1100°C (25 h in $^{16}O_2$ followed by 50 h in $^{18}O_2$) and they were then SIMS depth profiled. The depth pro-

filing measurements were conducted using the Atomika 6500 Ion Microprobe. A xenon source (Xe^+) was used (since we wished to measure oxygen) and a primary ion beam energy of 8 keV was selected to bombard the surface, at near normal incidence. The isotopic ratio or tracer enrichment parameter ν was plotted. $\nu = \frac{ir_{18} - g_1}{g_2 - g_1}$, g_1 and g_2 are the $^{18}O_2$ partial pressure in the first and second oxidation atmospheres respectively and $ir_{18} = \frac{^{18}O^-}{^{18}O^- + ^{16}O^-}$ the isotopic ratio derived from the secondary ion intensities of the ^{16}O and ^{18}O signals. The depth calibrated tracer enrichment (Fig. 35) revealed an area of high tracer enrichment at the gas–oxide interface which represents $^{18}O_2$ surface exchange. This tapers off to a plateau region with a tracer enrichment value of 0.05 and represents a region of fast inward oxygen diffusion via a grain boundary diffusion mechanism. It is interesting to note that the tracer enrichment does not fall to zero given that any background enrichment has already been accounted for in the measurement. By monitoring the ratio of oxygen isotopes we eliminate SIMS effects such as charging. This may correspond to the tracer having exchanged into the previous oxide grains or formed a new phase within the previous oxides grain boundaries. Such behaviour is as predicted by others, who have performed such two stage isotopic tracer experiments on alumina forming alloys. The tracer enrichment value then increases to a plateau with a ν-value of 0.45, which indicates a region of new oxide growth within the existing oxide. At the oxide-metal interface the tracer enrichment value begins to fall again and the noise in the rising tail of the profile is characteristic of profiling into the coating substrate.

2.9. Biomaterials

The application of SIMS, and other analytical techniques, to biomaterials has seen a very significant rise in the last few years. SIMS can be used to measure isotopes, as seen for example in the previous example, and deuterium and carbon 13 are potentially very useful species in bio-materials studies. Recent work reviewing the application of TOF-SIMS to the study of biomaterial surfaces such as implants have been reviewed by Belu [61]. The application of SIMS to the mapping of drug up-take in cellular structures has been described by Clerc [62]. Sample preparation techniques are described as are methods of detection which are accomplished indirectly by detecting a 'tag' isotope either naturally present or introduced by labeling, (usually N-15 and C-14). Another important review paper is given by Fragu [63] who discusses the measurement of anti-tumour drugs in histological sections using SIMS. Detection is dependent on the presence of chemical elements in the drug structure with species such as (F, Br, I) used to monitor the presence of drugs in the cell structure. Recently Lockyer has reviewed the progress in cellular analysis using TOF-SIMS [64].

2.10. SIMS in education

One of the rate limiting steps in the take up and application of any analytical technique is awareness. For many years, all the materials students at Imperial College have had hands on experience of electron microscopy and X-ray diffraction. Recently we have introduced a SIMS problem based learning exercise into our undergraduate curriculum [65]. This exercise involves the use of the Millbrook mini-SIMS instrument [66] for with this instrument the serious

Figure 34 (a) A 18th century ladies riding jacket from the collection at the V&A museum. The silver embroidery has been cleaned with a Nd:YAG laser, at 532 nm at a fluence of 2 Jcm^{-2}. (b) A close up of the silver thread showing a cleaned area next to an uncleaned area. (c) A Static SIMS spectrum from the Millbrook mini-SIMS indicating that salts are a significant source of contamination, and also showing some evidence of hydrocarbon contamination. (d) The intensities of some of the major peaks, before and after cleaning, relative to the intensity of the silver peak (Ag^+). (Continued on next page.)

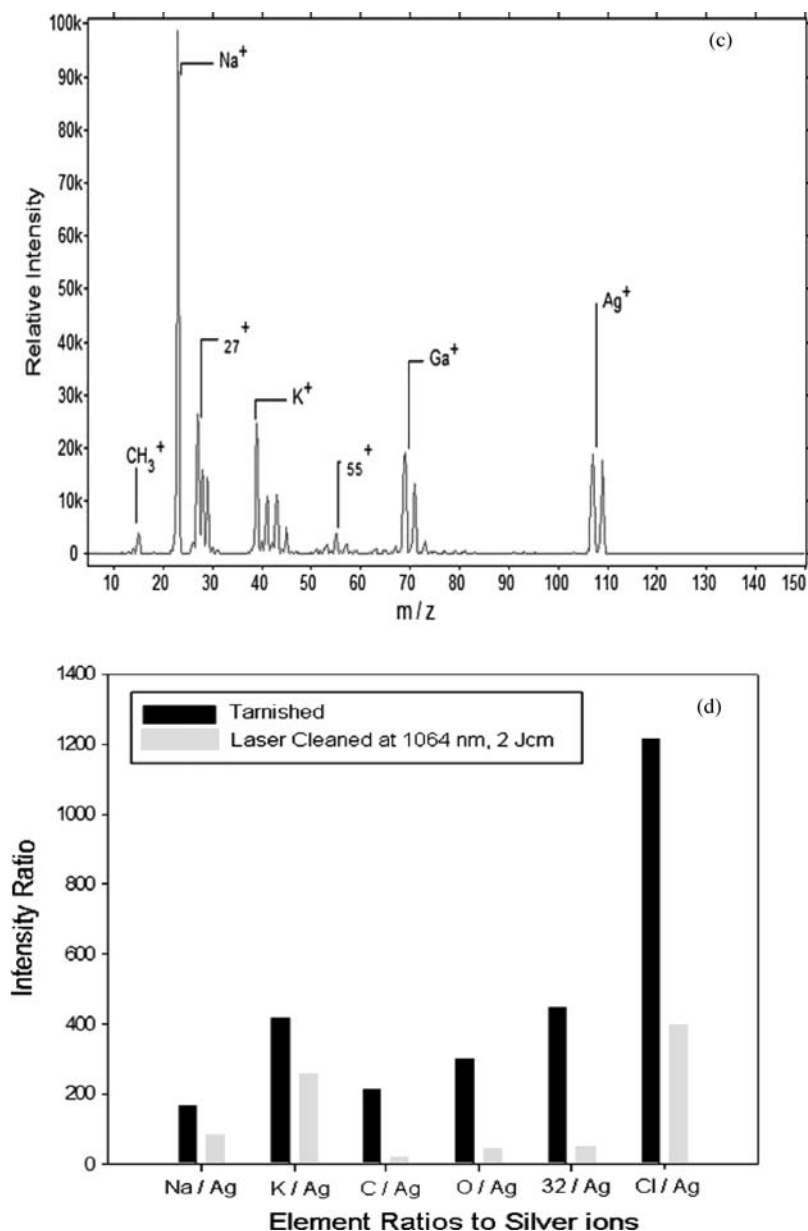

Figure 34 (Continued).

impediments of expense and complexity have been overcome by miniaturization and enhanced computer control. The main concept areas of sputtering and secondary ion production for surface chemical analysis are demonstrable in the briefest of laboratory sessions to students who have little background in SIMS. Within one afternoon the undergraduate students are introduced to the sample loading, generation of secondary ion mass spectra, secondary electron and secondary ion imaging, data interpretation, charge compensation and issues associated with quantification. Key concepts are introduced through a serious of case studies on molybdenum oxide (positive and negative secondary ion mass spectra), the copper grid (focusing of the primary ion beam) and silicon (static SIMS dose) and PTFE tape (charge compensation). The PBL exercise involves reverse engineering of the materials used on the blade of a razor (Fig. 36). Many of these students go on to use one of our SIMS instruments in their final year long project.

3. Conclusions

Secondary Ion Mass Spectrometry is a mature surface analysis technique that is finding a broad range of applications in materials science. The key attributes of this technique are its very high sensitivity (parts per billion in

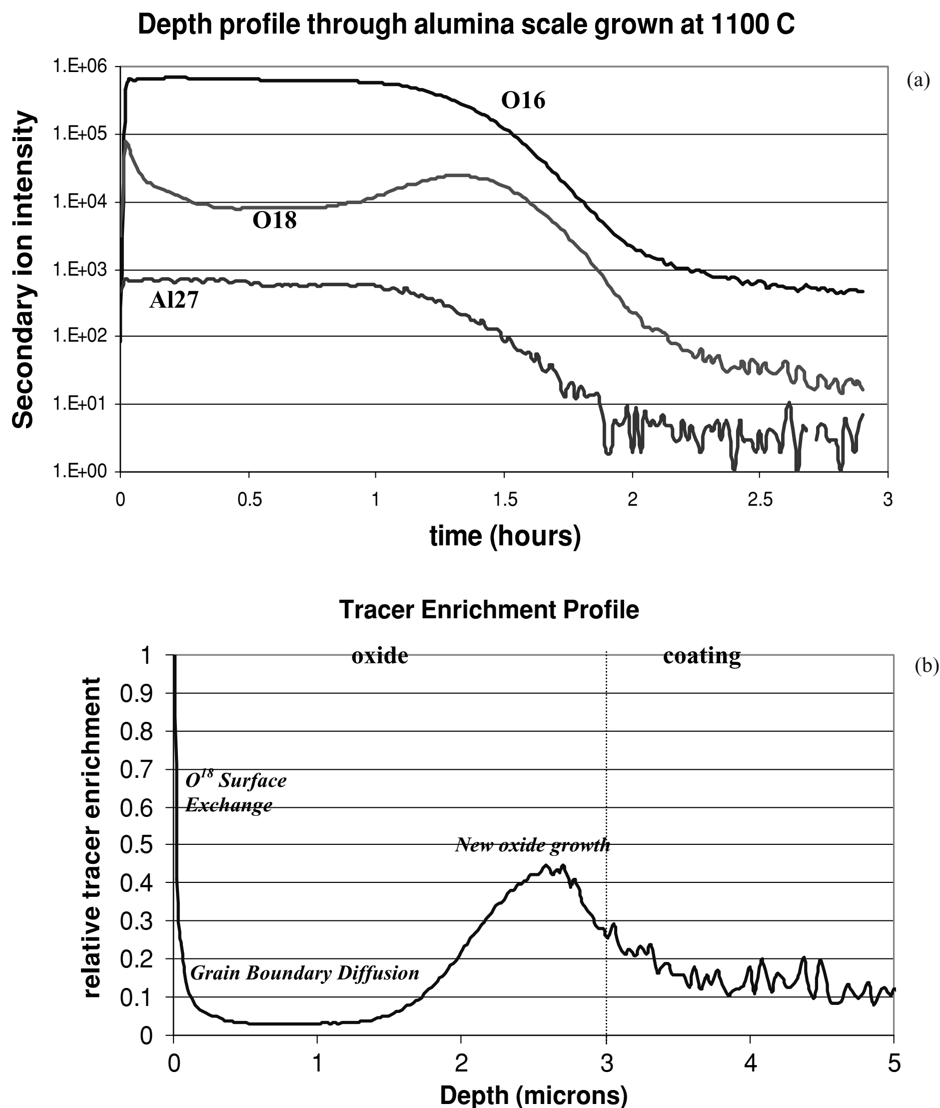

Figure 35 (a) A Depth Profile of a Platinum Aluminide Coating on a Superalloy Substrate grown at 1100°C for 25 h in $^{16}O_2$ followed by 50 h in $^{18}O_2$. (b) The tracer enrichment profile shows the relative tracer enrichment above background for oxygen 18 and indicates the mechanisms operating during the $^{18}O_2$ oxidation phase.

favorable cases) together with its excellent spatial resolution. Ultra-low energy SIMS depth profiling can achieve depth-resolutions of less than one nanometre so that ultra-slow changes to the surface of a material, for example oxidation, diffusion and corrosion, may be monitored without the need for accelerated ageing. A rate of change of 0.3 nm per day, corresponding to one millimetre every 10 millennia, may be measured. In the imaging mode SIMS can achieve lateral resolutions better than 50nm with good sensitivity, so that localized chemistry, for example around inclusions and close to grain boundaries may be assessed. Depth profiling and imaging can be combined to yield very powerful three-dimensional chemical maps. In the Static SIMS mode the resolution is essentially the information depth of the technique, a few monolayers.

The development of high mass primary ion species such as C_{60} are opening up the possibility of low damage analysis of bio-materials and polymers. A number of instruments are available with particular strengths and weaknesses and the advent of bench-top instrumentation is a welcome development.

The fifteenth biannual SIMS conference, SIMS XV (Manchester, September 2005) (http://www.meeting.co.uk/simsxv/) received a record number of abstracts so it is clear that SIMS is a technique with a compelling future.

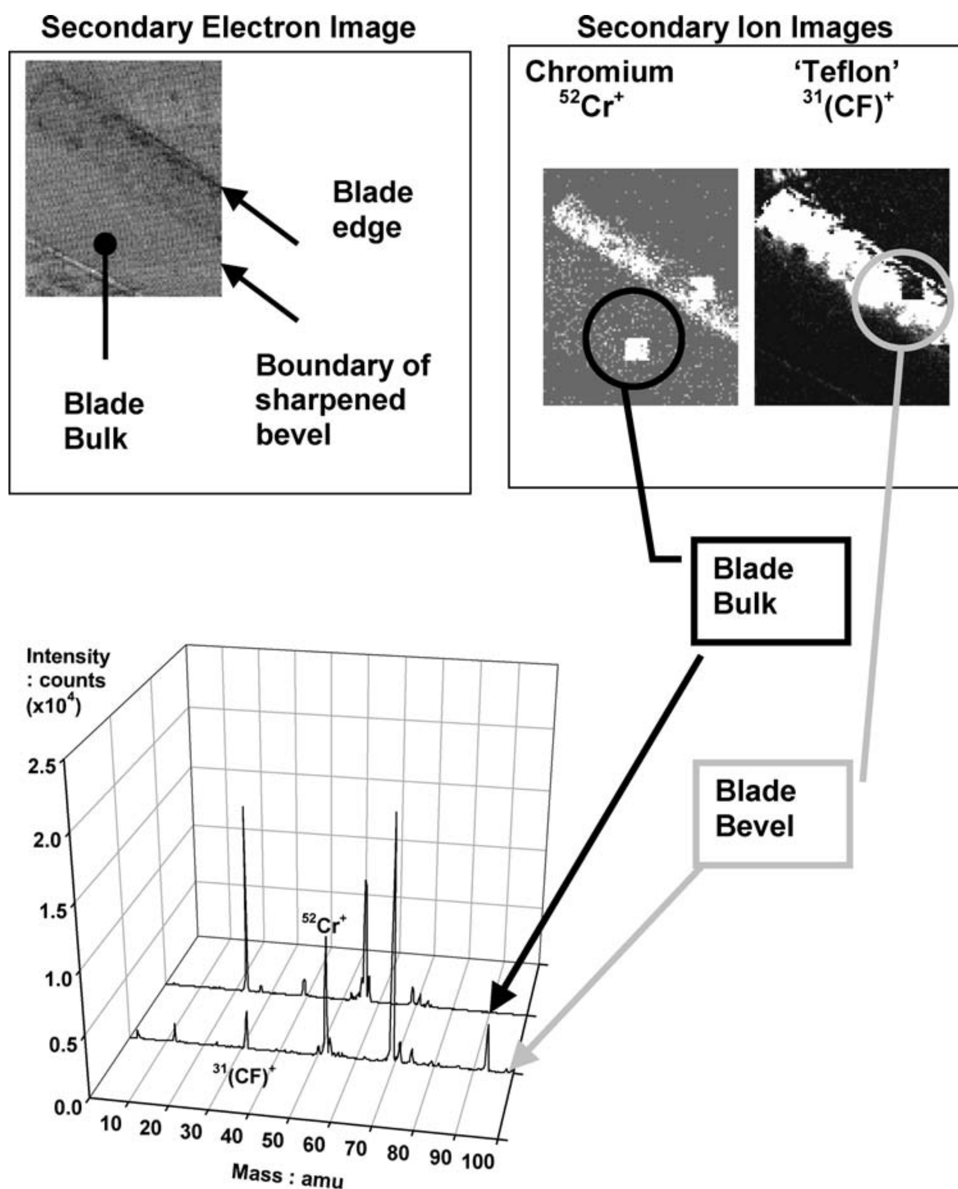

Figure 36 Secondary ion and electron images of the razor blade generated in the Millbrook system. Comparative secondary ion mass spectra from the Teflon and the Steel are shown.

Acknowledgements

I am very grateful to my colleagues Professor Mark Dowsett and Richard Chater, for their help and assistance with much of the work in this paper. Likewise I am grateful for the help and assistance, as well as experimental data, provided by my industrial partners, Dr. Hans-Ulrich Ehrke at FEI-Munich (now Cameca), Mr. Colin Helliwell and Dr. Birgit Hagenhoff at ION TOF (Munster), Dr. John Eccles at Millbrook Instruments and Dr. Rowland Hill at Ionoptika.

References

1. FEI, Brukmannring 40, 85764 Oberschleissheim, Munich, Germany, www.feicompany.com now http://www.cameca.fr/.
2. ION TOF GmbH, Gievenbecker Weg 15, D-48149 Munster, Germany, www.iontof.com.
3. http://www.srim.org/
4. W. VANDERVORST and F. R. SHEPHERD, *J. Vac. Sci. Technol. A* **5** (1987) 313.
5. S. C. C. WONG, R. HILL, P. BLENKINSOPP, N. P. LOCKYER, D. E. WEIBELAND and J. C. VICKERMAN, *Appl. Surf. Sci.* **203** (2003) 219.
6. J. J. THOMSON, *Philos. Mag.* (1910) 752.
7. S. HOFMANN, *Philos. Trans. Royal Soc. A* **362**(55–75) (2004) 1814.
8. K. WITTMAACK, *Vacuum* **34**(1/2) (1984) 119.
9. M. TOMITA, F. TAKAHASHI and F. Y. HOMMA, *Nucl. Instrum. Phys.* **85**(1–4) (1994) 399.
10. Ionoptika Ltd., Epsilon House, Chilworth Science Park, Southampton, SO16 7NS, UK. www.ionoptika.com.
11. Secondary Ion Mass Spectrometry, "A Practical Handbook for Depth Profiling and Bulk Impurity Analysis," R. G. Wilson, F.A. Stevie and C.W. Magee (John Wiley and Sons, 1989) ISBN 0-471-51945-6.

12. D. PHINNEY, "Semi-Quantitative Analysis of Microstructures by Secondary Ion Mass Spectrometry," in the Proceedings of EMAS 2005 (Florence, 2005) p. 73.
13. D. S. MCPHAIL and S. LITTLEWOOD, in SIMS VIII, edited by A. Benninghoven, K.T.F. Janssen, J. Tumpner and H.W. Werner (John Wiley, 1992, ISBN 0-471-93064-4) p. 407.
14. The International Roadmap for Semiconductors 2004 update, http://www.itrs.net/Common/2004Update/2004Update.htm.
15. M. G. DOWSETT, *Appl. Surf. Sci.* **203** (2003) 203.
16. Cameca France, 103 Boulevard Saint Denis, BP 6, 92403 Courbevoie cedex France, http://www.cameca.fr/.
17. G. GILLEN, R. LAREAU, J. BENNETT and F. STEVIE, SIMS XI: Proceedings of the 11th International Conference on Secondary Ion Mass Spectrometry, 'Secondary Ion Mass Spectrometry SIMS XI' (John Wiley and Sons, 1998, ISBN: 0-471-97826-4).
18. A. BENNINGHOVEN, P. BERTRAND, H. N. MIGEON and H. W. WERNER, SIMS XII: Proceedings of the 12th International Conference on Secondary Ion Mass Spectrometry 'Secondary Ion Mass Spectrometry SIMS XII', (Elsevier, 2000, ISBN 0-444-50323-4).
19. SIMS XIII: Proceedings of the Thirteenth International Conference on Secondary Ion Mass Spectrometry and Related Topics, Benninghoven, Applied Surface Science, 203 (2003) p. 203.
20. A. BENNINGHOVEN, J. L. HUNTER, JR. B. W. SCHUELER, H. E. SMITH and H. W. WERNER, SIMS XIV, Proceedings of the Fourteenth International Conference on Secondary Ion Mass Spectrometry and Related Topics (Applied Surface Science, 2004).
21. A. BENNINGHOVEN, F. G. RUDENAUER and H. W. WERNER, Secondary Ion Mass Spectrometry (John Wiley and Sons, 1987, ISBN 0-471-01056-1).
22. J. C. VICKERMAN, A. BROWN and N. M. REED, Secondary Ion Mass Spectrometry (Oxford Science Publications, Oxford, 1989, ISBN 0-19-855625-X).
23. J. C. VICKERMAN, D. BRIGGS and A. HENDERSON, The Static SIMS Library (IM Publications, 2002, ISBN 0-9537848-5-1).
24. J. C. VICKERMAN and D. BRIGGS, ToF-SIMS: Surface Analysis by Mass Spectrometry, IM publications, 2002, ISBN 1-901019-03-9).
25. http://www.simsworkshop.org/links.htm.
26. M. G. DOWSETT, N. S. SMITH, D. R. BRIDGELAND, A. C. LOVEJOY and P. PENDRICK, in Secondary Ion and Mass Spectrometry SIMS XI, edited by A. Benninghoven, B. Hagenhoff, and H. W. Werner (John Wiley and Sons, 1998, ISBN: 0-471-97826-4) p. 367.
27. J. BELLINGHAM, M. G. DOWSETT, E. COLLART and D. KIRKWOOD, *Appl. Surf. Sci.* **203** (2003) 831.
28. R. B. BEALL, J. B. CLEGG, J. CASTAGNE, J. HARRIS, J. J. MURRAY and R. C. NEWMAN, *Semiconductor Sci. Technol.* **4** (1989) 1171.
29. G. P. BEYER, D. S. MCPHAIL, A. KHAN and M. GHISONI, "Applications Of Particle And Laser Beams In Materials Technology NATO ASI Series" edited by P. Misaelides (Kluwer Academic Publishers, 1995) 151.
30. G. P. BEYER, D. S. MCPHAIL and M. GHISONI, "SIMS IX", edited by A. Benninghoven, Y. Nihei, R. Shimizu and H.W. Werner (John Wiley and Sons, 1994) 682.
31. R. LAREAU, in "Secondary Ion Mass Spectrometry SIMS VI," edited by A. Benninghoven, A.M. Huber and H.W. Werner (Wiley, New York, 1988, ISBN 0-471-91832-6) p. 437.
32. J. HERNIMAN, J. S. YU and A. E. STATON BEVAN, *Appl. Surf. Sci.* **52**(4) (1991) 289.
33. C. M. HSU and D. S. MCPHAIL, *Nuclear Instruments and Methods in Physics Research* **B-101**(4) (1995) 427.
34. C. M. HSU, V. K. M. SHARMA, M. J. ASHWIN and D. S. MCPHAIL, *Surface and Interface Analysis*, **23**(10) (1995) 665.
35. K. P. JOHANSEN, D. S. MCPHAIL and S. FEARN, in "Microscopy of Semiconducting Materials, Proceedings of Institute of Physics Confernece Series (164)" 1999, p. 465.
36. S. FEARN and D. S. MCPHAIL, accepted for publication in the Journal of Applied Surface Science (January 2005).
37. N. J. MONTGOMERY, J. L. MACMANUS-DRISCOLL, D. S. MCPHAIL, R. J. CHATER, B. MOECKLY and K. CHAR, *Thin Solid Films* **317**(1/2) (1998) 237.
38. A. LODDING, H. ODELIUS, D. E. CLARK and L. O. WERME, *Mikrochimica Acta* **11** (1985) 145.
39. G. G. WICKS, 'Nuclear Waste Glasses: Corrosion Behaviour and Field Tests' in "Corrosion of Glass, Ceramics, and Superconductors" edited by D. E. Clark and B. K. Zoitos (Noyes Publication, 1991).
40. S. E. T. HOGG, D. S. MCPHAIL, P. S. ROGERS and V. L. OAKLEY, 'Mono-Functional Organosilanes as Candidates for Treatments of Crizzling in Glasses' in "the Proceedings of the ICOM-CC Working Group", edited by Alice. B. Paterkis (1998) p. 53.
41. S. FEARN, D. S. MCPHAIL and V. OAKLEY, *Appl. Surf. Sci.* **231/232C** (2004) 510.
42. J. L. RYAN, '*The Atmospheric Deterioration of Glass: Studies of Decay Mechanisms and Conservation Techniques*', PhD Thesis, University of London, 1996.
43. V. OAKLEY, '*Vessel Glass Deterioration at the Victoria and Albert Museum: Surveying the Collection*', The Conservator, 14 (1990) p. 30.
44. D. E. CLARK, L. L. HENCH and C. G. PANTANO, '*Corrosion of Glass*', New York, Books for Industry (1976). /
45. M. DOWSETT and A. ADRIEANS, *Nucl. Instr. Methods Phys. Res.* **B 226** (1–2) (2004) 226.
46. Why Stainless Steel Corrodes, M.P. Ryan, D.E. Williams, R.J. Chater, B.M. Hutton and D.S. McPhail, Nature 415 (6873) (14th February 2002) p. 770.
47. E. E. REES, D. S. MCPHAIL, M. P. RYAN, M. G. DOWSETT and J. KELLY, *Appl. Surf. Sci.* **203/204** (2003) 660.
48. K. SIERADZKI and R. C. NEWMAN, *J. Electrochem. Soc.* (1984) 1979.
49. R. J. CHATER, G. A. GRAHAM, D. S. MCPHAIL and A. T. KEARSLEY, *Appl. Surf. Sci.* **231/232** (2004) 893.
50. G. A. GRAHAM, R. J. CHATER, D. S. MCPHAIL, A. T. KEARSLEY, M. R. LEE, S. KETTLE and I. P. WRIGHT, *Meteoritics & Planetary Science* **37**(7) (2002) A. 56.
51. G. A. GRAHAM, P. G. GRANT, R. J. CHATER, A. J. WESTPHAL, A. T. KEARSLEY, C. SNEAD, G. DOMINGUEZ, A. L. BUTTERWORTH, D. S. MCPHAIL, G. BENCH and J. P. BRADLEY, *ibid.* **39**(9) (2004) 1461.
52. G. A. GRAHAM, A. T. KEARSLEY, A. L. BUTTERWORTH, P. A. BLAND, M. J. BURCHELL, D. S. MCPHAIL, M. J. BURCHELL, R. CHATER, M. M. GRADY, I. P. WRIGHT and C. T. PILLINGER, *Advances in Space Research* **34** (2004) 2292.
53. R. J. CHATER, S. CARTER, J. A. KILNER and B. C. H. STEELE, *Solid State Ionics*, **53–56**, (1992) 859.
54. K. HALLETT, D. THICKETT, D. S. MCPHAIL and R. J. CHATER, *Applied Surface Science* **203–204** (2003) 789.
55. M. SOKHAN, P. GASPAR, D. S. MCPHAIL, A. CUMMINGS, L. CORNISH, F. HARTOG, C. HUBBARD, V. OAKLEY and J. F. MERKEL, in Journal of Cultural Heritage 4, no. 1001 (Elsevier Science, January 2003) p. 230.
56. Lynton Lasers Ltd. Lynton House, Manor Lane, Holmes Chapel, Cheshire. CW4 8AF Tel: +44 (0)1477 536 977, Fax: +44 (0)1477 536 978. http://www.lynton.co.uk/.
57. D. S. MCPHAIL, M. SOKHAN, E. E. REES, B. CLIFF, A. J. ECCLES and R. J. CHATER, *Appl. Surf. Sci.* **231–232** (2004) 967.
58. D. P. GARRIGA-MAJO, R. J. CHATER, D. MCPHAIL and B. A. SHOLLOCK, *International Journal of Inorganic Materials* **1** (1999) 325.
59. A. A. ALIBHAI, D. S. MCPHAIL and B. A. SHOLLOCK, in SIMS 12 (see 14 above) (2000) p. 867.

60. A. A. ALIBHAI, D. P. GARRIGA-MAJO, B. A. SHOLLOCK and D. S. MCPHAIL, Superalloys 2000, 684 (ISBN 0-87339-477-1) (2000) p. 675.
61. A. M. BELU, D. J. GRAHAM and D. G. CASTNER, *Biomaterials*, **24** (2003) 3635.
62. J. CLERC, C. FOURRE and P. FRAGU, *Cell Biology International*, **21**(10) (1997) 619.
63. P. FRAGU and E. KAHN, *Micropscopy Research and Techniques*, **36**(4) (1997) 296.
64. N. P. LOCKYER and J. C. VICKERMAN, *Applied Surface Science* **231**(15) (2004) 377.
65. R. J. CHATER and D. S. MCPHAIL, *Applied Surface Science*, **231–232** (2004) 141.
66. Millbrook Instruments Ltd, Blackburn, BB1 5QB, UK : Web address at http://www.millbrook-instruments.com.